Metallosupramolecular Chemistry of Novel Chiral *closo-o*-Carboranylalcohol Pyridine and Quinoline Ligands: Syntheses, Characterization, and Properties of Cobalt Complexes

Florencia Di Salvo,[†] Francesc Teixidor,[†] Clara Viñas,[†] José Giner Planas,*,[†] Mark E. Light,[‡] Michael B. Hursthouse,[‡,±] and Núria Aliaga-Alcalde[§]

[†]Institut de Ciència de Materials de Barcelona (ICMAB-CSIC), Campus UAB, 08193 Bellaterra, Spain

[‡]School of Chemistry, University of Southampton, Highfield, Southampton SO171BJ, United Kingdom

[±]Department of Chemistry, Faculty of Science, King Abdulaziz University, Jeddah 21588, Saudi Arabia

[§]ICREA Researcher (ICREA: Institució Catalana de Recerca i Estudis Avançats) and Departament de Química Inorgànica, Universitat de Barcelona (UB), Diagonal 645, 08028 Barcelona, Spain

ⓢ *Supporting Information*

ABSTRACT: The cobalt(II) complexes $CoCl_2(LOH)_2$ (LOH = 1-[R(hydroxy)methyl]-2-R′-1,2-dicarba-*closo*-dodecaborane (R′ = H or Me; R = 2-pyridyl **3a** or **4a**, 3-pyridyl **3b** or **4b**, 4-pyridyl **3c** or **4c**, 2-quinolyl **3d** or **4d**, 4-quinolyl **3e** or **4e**)) and $CoCl_2(LOH)_4$ (**5**, R′ = H; R = 4-pyridyl) were synthesized and characterized. Deprotonation of alcohol in **3a** afforded the square-planar complex $Co^{II}(LO)_2$ (**6**) that oxidized slowly in solution and under air to give the cobaltacarborane complex $Co^{III}\{(\eta^5\text{-}C_2B_9H_{10})(CHOH)(\eta^1\text{-}NC_5H_4)\}(\eta^2\text{-}NC_5H_4COO)$ (**7**). Crystal structures for **3a**, **3a·2MeOH**, **3b**, **3e**, **4c**, **4e**, **5**, **6**, and **7** have been determined by X-ray diffraction (XRD). Molecular structures show octahedral (**3a**, **3a·2MeOH**, **5**), tetrahedral (**3b**, **3e**, **4c**, **4e**), and square-planar (**6**) coordination around Co^{II} centers, whereas 2-pyridyl and quinolyl ligands favor a bidentate *N,O*-coordination mode and 3- and 4-pyridyl and quinolyl ligands favor a monodentate *N*-coordination. The supramolecular structures are dominated by intermolecular O−H···Cl/O hydrogen bonds and π−π interactions in the case of tetrahedral complexes. The magnetic properties of **3a−c** were investigated in the temperature range 2−300 K by means of $\chi_M T$, which corroborated coordination numbers and geometries as well as provided information on the supramolecular interactions among neighboring molecules for all three compounds. Complex **3a** shows solvent accessible channels running parallel to the hydrogen bonding network and is able to uptake methanol vapors to convert into **3a·2MeOH**. The structure of **3a** is related to that for **3a·2MeOH** by rotation of complex molecules within the 1D O−H···Cl hydrogen bonding networks and insertion of methanol into it.
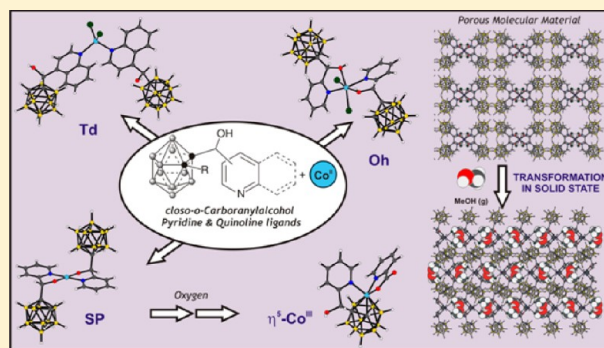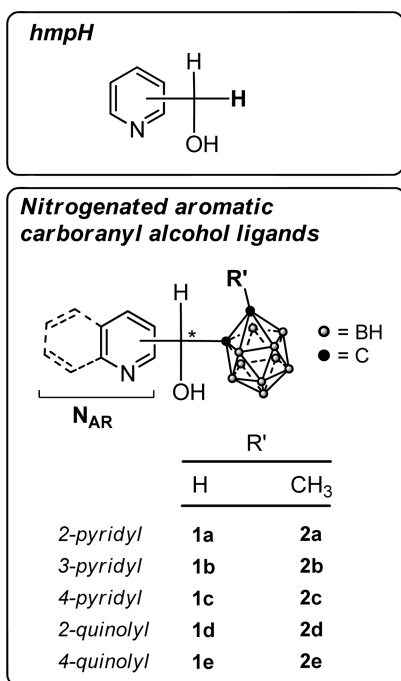
INTRODUCTION

In recent decades, the design of hybrid functional materials has been a matter of special interest because of their potential applications in a number of areas.[1] A well-known approach for the preparation of such systems is the synthesis of organic−inorganic frameworks where transition metal ions and nitrogen containing heterocyclic ligands have proved useful for the construction of solid-state architectures and inorganic crystal engineering.[2] In particular, pyridyl based ligands have been successfully used for constructing a wide array of architectures with applications ranging from gas storage in porous frameworks to novel luminescence or magnetic materials.[3] The assembly of porous materials from organic ligands and metal ions to generate new supramolecular architectures is challenging.[4] There are many such materials which self-assemble around solvent-containing cavities to form solid state structures. In such cases, the initial criterion for a potentially useful system will be the robustness of the molecular architecture to the removal of solvent, and the consequent preservation of the cavity of potential value for application to gas storage. The increasing need for evolved systems and demanding assemblies has led to the emergence of heterodonating functions,[3a,f] among which *N,O* ligands such as (hydroxymethyl)pyridines (hmpH) are candidates (top of Scheme 1). These simple alcohol pyridines have proved to be successful building blocks for the self-assembly of metallosupramolecular architectures with exciting physical properties.[5] The possibility for placement of the methylalcohol moiety at the 2-, 3-, or 4-position with respect to the pyridine nitrogen, which usually coordinates to

Scheme 1. Carboranylmethylalcohols and Related hmpH Ligands

hmpH

Nitrogenated aromatic carboranyl alcohol ligands

○ = BH
● = C

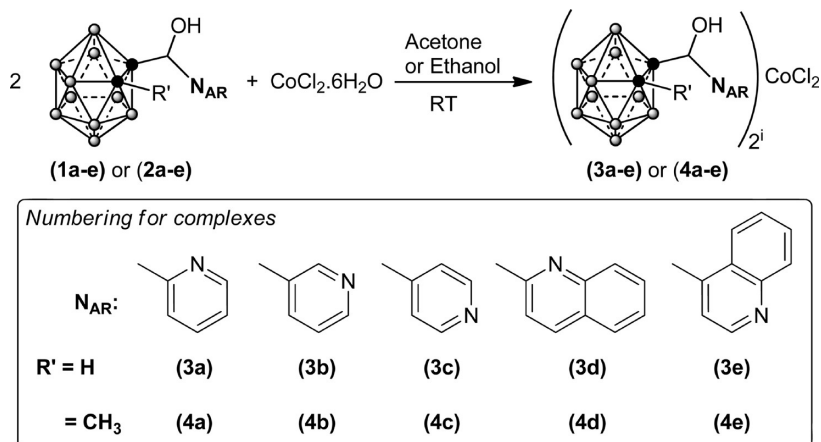|	R'	
	H	CH$_3$
2-pyridyl	**1a**	**2a**
3-pyridyl	**1b**	**2b**
4-pyridyl	**1c**	**2c**
2-quinolyl	**1d**	**2d**
4-quinolyl	**1e**	**2e**

the metal center, is a key feature that allows these ligands to support a whole family of supramolecules of different nature. From the three isomers, 2-hmpH is the most studied, since, unlike the 3- and 4-isomers, the alcohol group can act as a second coordination unit. 2-HmpH is known to act as a bidentate ligand, forming 5-membered chelate rings with metals via their *N,O* donor atoms. The alcohol function also provides the opportunity of stepwise deprotonation before or upon coordination, leading to a large diversity of complexes and structures. Thus, this ligand (2-hmpH) exhibits very rich coordination chemistry, forming a diverse range of mononuclear, dinuclear, and polynuclear complexes, and polymeric structures.[5a−e] Heterobidentate ligands of this type offer several advantages over traditional symmetrical bidentate ligands by creating steric and electronic asymmetry and chirality at the metal centers.[6] It is, however, surprising that almost no chiral derivatives of 2-hmpH have been investigated.[5c]

We have recently described the synthesis and molecular and supramolecular characterization of a series of new nitrogenated aromatic carboranyl alcohols obtained from the reaction of the monolitiated salt of the methyl-*o*-carborane or *o*-carborane with different aldehydes (**1a−e** and **2a−e**, respectively; bottom of Scheme 1).[7] These molecules, that are prepared in very good yields from one pot reactions and from readily available starting materials, can be regarded as hmpH ligands where one of the H atoms at the −CH$_2$− position of the alcohol arm has been replaced by a carboranyl fragment. The success of this procedure has opened a new door toward the synthesis of very attractive, yet unexplored, carborane based transition metal complexes. The high thermal and chemical stability, hydrophobicity, acceptor character, ease of functionalization, and three-dimensional nature of the icosahedral carborane clusters make these new molecules valuable ligands in coordination chemistry.[8] In addition, the asymmetry and chiral nature of **1a−c** and **2a−c**, together with their ability for establishing H-bonds,[7b,c] will provide intrinsic features to the final metal complexes, allowing unique fingerprints. Herein, we report our initial studies of the metallosupramolecular chemistry of these ligands, which includes the synthetic procedures, molecular and supramolecular structures, and magnetic properties of new cobalt complexes. This work highlights the remarkable versatility of the coordination and supramolecular chemistry of carboranyl alcohol ligands and extends our initial studies on crystal engineering of icosahedral heteroborane clusters to that of metal−organic−inorganic architectures. The present report includes an interesting intrinsically porous molecular material, whose porosity is triggered by self-assembly into the solid state and by the presence of the carboranyl fragment.

■ RESULTS AND DISCUSSION

Synthesis and Characterization. Complexes of the type [CoCl$_2$(LOH)$_2$] (**3a−c** and **4a−c**; Scheme 2) were synthesized by mixing ethanol or acetone solutions of the pyridine based carboranylalcohol ligands (LOH: **1a−c** and **2a−c**; Scheme 1) with CoCl$_2$·6H$_2$O in a 2:1 ratio under aerobic conditions. Formation of the complexes was evidenced by a rapid color intensification of the solutions (few seconds). Workup of the reactions gave the corresponding complexes in high yields as violet (**3a**, **4a**) or blue solids (**3b−c**, **4b−c**). The stoichiometry of the latter pyridine based carboranylalcohol complexes was

Scheme 2. Synthesis of New Complexes

Numbering for complexes

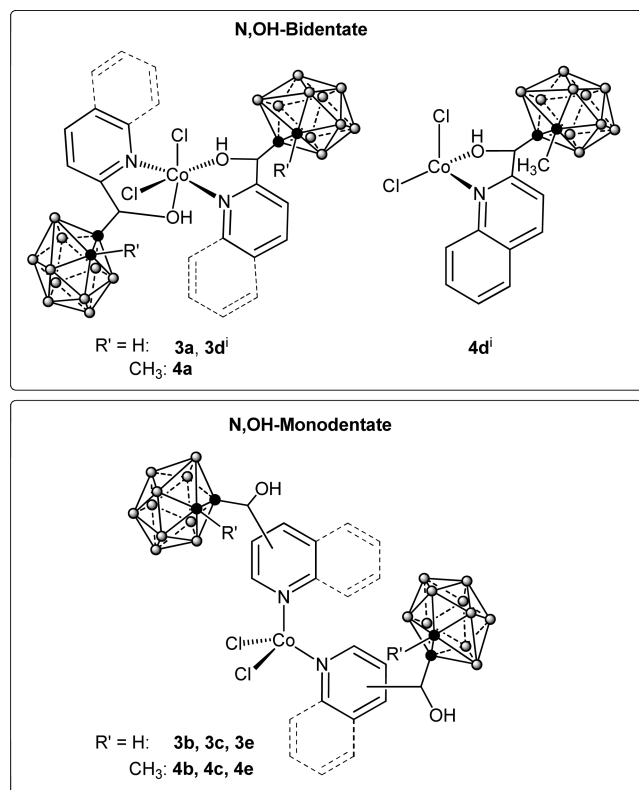|					
N$_{AR}$:					
R' = H	**(3a)**	**(3b)**	**(3c)**	**(3d)**	**(3e)**
= CH$_3$	**(4a)**	**(4b)**	**(4c)**	**(4d)**	**(4e)**

[i]Except for **3d** and **4d**, which show a ligand to metal ratio of 2 and/or 1 (see text).

initially confirmed by elemental analysis, which shows a ligand to $CoCl_2$ ratio of 2:1 (Scheme 2). The straightforward methodology and the stability of these compounds in solution and under air for several days are remarkable.

As mentioned in the Introduction, the carboranyl cages are rather bulky, and this poses a challenge for the coordination chemistry of these ligands. And bulkiness is certainly increased in the case of the quinolyl based carboranylalcohol ligands (**1d–e** and **2d–e**; Scheme 1). Thus, the reactions of $CoCl_2 \cdot 6H_2O$ with 2-quinolyl (**1d** or **2d**) or 4-quinolyl (**1e** or **2e**) based ligands in a 2:1 ratio afforded greenish (**3d**, **4d**) or blue solids (**3e**, **4e**) as shown in Scheme 2. Elemental analyses of the latter, having the 4-quinolyl moiety, agree with the molecular formula $[CoCl_2(LOH)_2]$, in accordance with the pyridyl based ligands. The situation is, however, more complicated in the case of the 2-quinolyl based complexes (**3d** and **4d**). The bulkier nature of these ligands, together with the possibility to be coordinated through both nitrogen and oxygen atoms to act as *N,O* chelates (*vide infra*), made the formation of the $[CoCl_2(LOH)_2]$ complexes less favorable. Thus, whereas elemental analysis of solid samples for **4d** agreed with a $[CoCl_2(LOH)]$ complex, that for **3d** seems to correspond to mixtures of both possible complexes $[CoCl_2(LOH)_2]$ and $[CoCl_2(LOH)]$. This is consistent with the bulkier Me-*o*-carboranyl moiety in **4d**, which seems to impede the coordination of a second ligand. The structures for complexes **3a–b**, **3d**, **4c**, and **4e** have been confirmed by single crystal X-ray diffraction (XRD), and their details will be analyzed in the following sections. It is, however, useful to summarize at this point the coordination modes and stoichiometries found in the new complexes (Scheme 3).

Scheme 3. Coordination Geometries for the New Complexes

N,OH-Bidentate

R' = H: **3a**, **3d**[i]
CH₃: **4a**

4d[i]

N,OH-Monodentate

R' = H: **3b**, **3c**, **3e**
CH₃: **4b**, **4c**, **4e**

[i]Postulated structures.

As summarized in Scheme 3, the 2-substituted ligands coordinate through both the O and N, giving octahedral complexes. Bidentate coordination is not possible in the 3- and 4- derivatives, and therefore, they coordinate through the nitrogen and in a monodentate fashion, giving tetrahedral complexes as shown in the scheme. We additionally considered the possibility to make octahedral complexes from the 3- or 4-substituted ligands. In our hands, only the less sterically hindered ligand (**1c**, Scheme 1) crystallized from the reaction mixture of **1c** with anhydrous $CoCl_2$ in a 4:1 ratio to provide the octahedral complex $[CoCl_2(LOH)_4]$ (**5**).

Although all complexes are paramagnetic, NMR spectroscopy can be very informative.[9] ^1H, ^{13}C, and ^{11}B NMR experiments were performed in acetone solutions of the cobalt complexes and were also applied to monitor the reaction evolution through *in situ* NMR experiments. Such experiments confirmed that the *o*-carboranylmethanols react immediately after they are mixed with the cobalt salt with >99% conversion into the corresponding complex, based on the free ligand signals. Both ^1H and ^{13}C spectra were assigned on the basis of known pyridine based paramagnetic Co^{II} complexes.[10] NMR signals for the 2-pyridyl (**3a**, **4a**) and quinolyl (**3d**, **4d**) derivatives were found to be broader than that for the related 3- and 4-derivatives (**3b–c**, **3e**, **4b–c**, **4e**), so that only partial characterization was possible in the former complexes (Supporting Information). For the latter complexes, the number of observed signals at the NMR spectra equals the number of chemically nonequivalent atoms. In these cases, ^1H and ^{13}C NMR signals in acetone solutions spanned from 151 to 1 and 536 to 24 ppm, respectively. As an example, the protons of the 4-pyridyl fragment in **3c** H(2) and H(6) were observed as very broad signals at the largest downfield shift (∼146 ppm) while H(3) and H(5) protons appeared as a relatively sharp signal at 40.1 ppm. Signals for the CH, OH, and C*c*H protons (C*c*: carbon cage) appeared in the same area range as in the free ligands, showing a negligible influence of the paramagnetic cobalt center on these parts of the molecule. In general, the nearest nuclei to the cobalt exhibit the largest chemical shift as well as the greatest line broadening. Regarding the boron atoms from the cluster, they are apparently not affected by the metal, and therefore, $^{11}B\{^1H\}$ NMR spectra for all complexes, including that for the 2- pyridyl and quinolyl derivatives, were obtained and are consistent with a *closo*-icosahedral geometry for the boron cages.[5,11] A comparison of NMR spectra of the free ligands and their complexes is available in the Supporting Information. Solid state IR spectra for all compounds show diagnostic signals for the OH and BH stretching frequencies in the ranges 3400–3300 and 2617–2560 cm^{-1}, respectively. The IR frequencies for the OH bands are very broad, suggesting the existence of H-bond interactions between the OH proton and a proton acceptor center present in these molecules.

As mentioned above, deprotonation of alcohol-containing chelates such as, for example, 2-hmpH (Scheme 1, top) provides alkoxide groups, which are excellent bridging units that can favor the formation of high nuclearity products.[5a–f] Deprotonation experiments were done in the cobalt complex **3a**, having the *N,O* bidentate 2-pyridyl based carboranylalcohol ligand. Treatment of **3a** with potassium *tert*-butoxide (Bu^{t}OK) as the base in dry methanol and under inert atmosphere was followed by precipitation of KCl. Slow evaporation under inert atmosphere of the resultant pink-violet solution afforded the square-planar Co^{II} complex **6** as light violet crystals suitable for XRD analysis. The analysis confirmed that both bidentate

ligands in **3a** had lost their OH protons and that chloride atoms were also removed to afford the square planar complex **6** (Scheme 4). The molecular structure will be described below.

Scheme 4. Reactivity of 3a
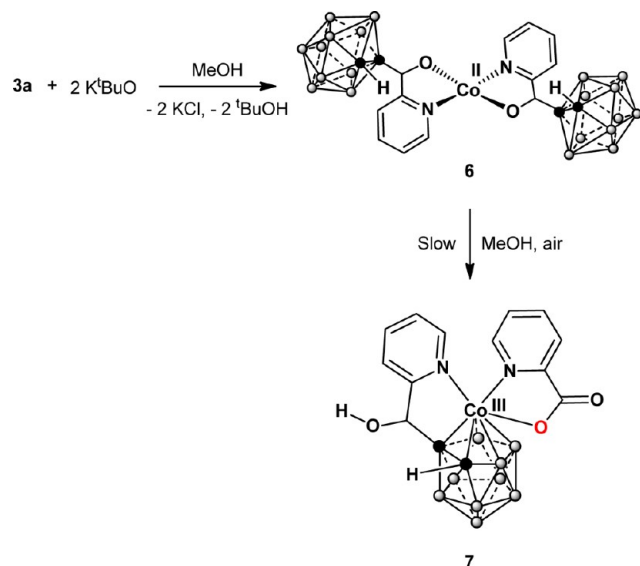
The absence of the alcohol function was also confirmed by FTIR. Interestingly, when readily formed complex **6** was left to evaporate slowly under air, instead of an inert atmosphere, bright blue crystals were obtained after several weeks. XRD analysis of the latter showed that an oxidative process has occurred with the formation of the cobaltacarborane complex **7** shown in the Scheme 5. In complex **7** a Co^{III} center is inserted into a *nido* cluster—from the degradation of ligand **1a**—to give a metallacarborane cluster with *closo*-[3,1,2-CoC_2B_9] geometry, and the pending pyridine ring is coordinated to the metal. Degradation of a *closo*-carboranyl moiety into its *nido* form and η^5-coordination of a metal to form a *closo*-metallacarborane are well-known to occur under the appropriate conditions.[12] What was more unexpected to us is that the remaining vacant sites in this complex are occupied by a deprotonated bidentate 2-pyridinecarboxylic acid. The latter is the result of C—C bond cleavage in ligand **1a** and oxidation of the alcohol moiety to a carboxylic acid one. The reaction is not optimized, but crystals of **7** are repeatedly formed when solutions of **6** are left in air.

Molecular Structures. The color observed for Co^{II} coordination complexes can be associated with their geometry. While blue solids are associated with tetrahedral geometries, green, pink, and/or violet can be associated with octahedral coordination environments.[13] Therefore, the colors of our complexes were taken as indicative of their different structures. Thus, we expected tetrahedral coordination geometries in the case of the blue $CoCl_2(LOH)_2$ solids (**3b–c**, **3e**, **4b–c**, and **4e**) whereas an octahedral coordination is most probably the reason for the violet solids (**3a** and **4a**). The greenish color for the 2-quinolyl derivatives **3d** and **4d** cannot, however, be unequivocally associated with their geometry. As mentioned above, elemental analysis of solid samples for **4d** agreed with a $CoCl_2(LOH)$ complex, whereas that for **3d** corresponded to mixtures of both possible octahedral $CoCl_2(LOH)_2$ and tetrahedral $CoCl_2LOH$ complexes. To verify geometries for all complexes, crystallization experiments were performed under different solvents and temperature conditions. In general, solutions of acetone

or ethanol or their mixtures gave crystals suitable for X-ray diffraction after slow evaporation of the solvent. Overall, we observed that complexes derived from the smaller *o*-carboranyl (rather than Me-*o*-carboranyl) alcohols and 3- and 4-substituted pyridine and quinoline derivatives, with the exception of **3a**, crystallized more easily. Thus, the structures for complexes **3a–b**, **3e**, **4c**, and **4e** have been confirmed by X-ray crystallography and are in agreement with their color in the solid state. The structures for an interesting methanol solvate of **3a** (**3a·2MeOH**) and complexes **5**, **6**, and **7** have also been solved by single crystal XRD (Figures 1–8). Crystal and data collection details can be found in Table 1 and the Experimental Section.

X-ray structure determination of complexes **3a** and **3a·2MeOH** (Figure 1) revealed distorted octahedral geometries, where each cobalt(II) center is coordinated by the nitrogen and oxygen atoms of two bidentate (2-pyridine)-(*o*-carboranyl)methanol ligands and two chloride atoms. In both complexes, the pyridine nitrogens are *trans*-positioned and the oxygen atoms of the chelating ligands and the chloride ions are in a *cis*-position. In addition, the molecular structure for **3a·2MeOH** shows the presence of two methanol molecules that act as hydrogen bond acceptors for both OH groups of the chelating ligands as shown in Figure 1. On the other hand, the cobalt(II) centers in complexes **3b**, **3e**, **4c**, and **4e** are tetrahedrally coordinated by two chloride atoms and two nitrogens of the pyridyl or quinolylcarboranylalcohol ligands that act as monodentate ligands (Figures 2–5). The same monodentate coordination of the 4-pyridyl ligand is observed in complex **5** (Figure 6), but in this case the molecular structure shows an octahedral coordination in which each cobalt ion is surrounded with four nitrogen atoms of the pyridine rings in the equatorial positions and two chlorides in the apical position. Selected bond lengths and angles of the complexes are given in Figures 1–6. Molecular structures for **3a–b**, **3e**, **4c**, **4e**, and **5** show bond lengths and angles consistent with those of related Co^{II} complexes.[14]

It is noteworthy to comment on the square planar complex **6**. The crystal structure for complex **6** shows a Co^{II}, sitting on an inversion center and lying within the {N_2O_2} plane. The geometry around the metal is clearly square-planar with a τ_4 parameter[15] 0.00 and no solvent molecule coordinated axially. The square-planar geometry seems to be stabilized by two intramolecular B—H⋯Co interactions (H⋯Co, 2.56(3) Å; BHCo, 121.1(2)°) from both carborane cages on the axial positions as shown in Figure 7. A search of the Cambridge Structural Database (V 5.33)[16] for Co^{II} complexes in a four-coordinate environment with τ_4 parameter <0.25 and bidentate N,O-ligands revealed only 12 complexes.[17] The Co—O and Co—N bond lengths and the bite angle of the ligand are comparable with the values observed for the related square planar geometry.[17]

As shown in Figure 8, in the cobaltacarborane complex **7**, the cobalt center Co(3) is η^5-bound to a *nido*-carboranyl ligand, η^1-coordinated to the nitrogen of the pyridine methyl alcohol tethered dicarbollyl ligand and a bidentate 2-pyridinecarboxylic acid. The two nitrogen atoms and one oxygen atom from the carboxylate ligand are arranged in a three-legged piano stool geometry. Bond lengths and angles are consistent with those of related metallacarborane complexes.[10a,b]

It is particularly interesting to compare the octahedral complex **3a** and its methanol solvated form **3a·2MeOH** (Figure 1). Both complexes show the same arrangement of ligands (same isomer out of five possibilities); however, the bond lengths and
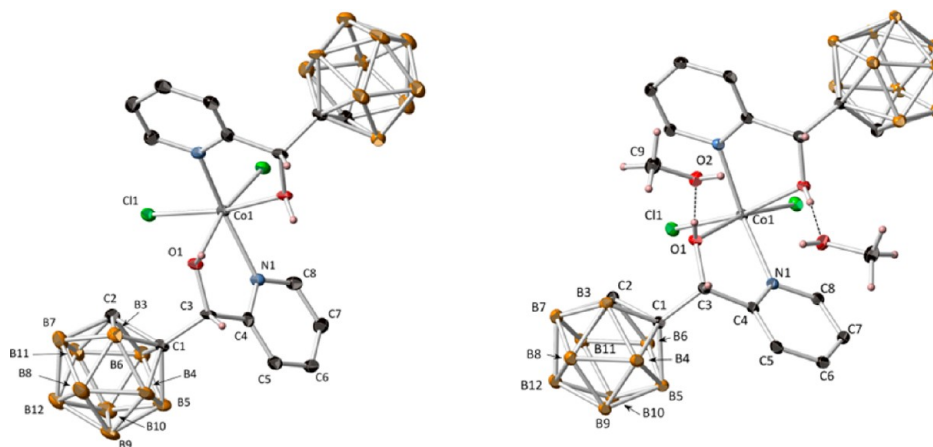
Figure 1. Molecular structures of **3a** (left) and **3a·2MeOH** (right); thermal ellipsoids set at 35% probability (selected hydrogen atoms are omitted for clarity). Selected interatomic distances (Å) and angles (deg): **3a**, Co1−N1 2.132(3), Co1−N1^i 2.132(4), Co1−O1 and Co1−O1^i 2.222(3), Co1−Cl1 and Co1−Cl1^i 2.3872(12), N1−Co1−N1^i 154.8(2), O1−Co1−Cl1^i and O1^i−Co1−Cl1 168.24(8) [$i = -x + \frac{1}{2}, -y, z$]; **3a·2MeOH**, Co1−N1 and Co1−N1^i 2.1355(17), Co1−O1 and Co1−O1^i 2.2535(15), Co1−Cl1 and Co1−Cl1^i 2.3804(6), N1−Co1−N1^i 142.12(9), O1−Co1−Cl1^i and O1^i−Co1−Cl1 169.15(4) [$i = -x + \frac{1}{2}, -y + \frac{1}{2}, z$].
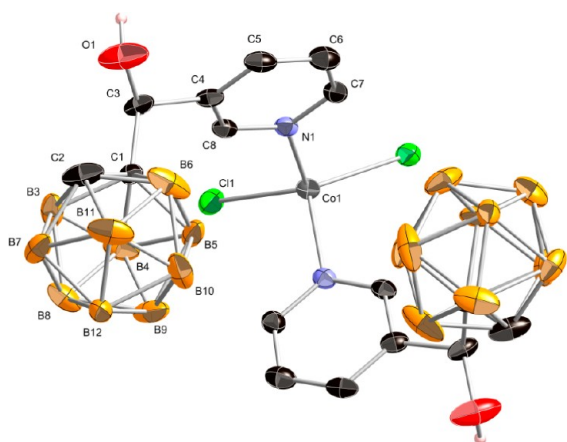

Figure 2. Molecular structure of **3b**; thermal ellipsoids set at 35% probability (selected hydrogen atoms are omitted for clarity). Selected interatomic distances (Å) and angles (deg): Co1−N1 and Co1−N1^i 2.038(4), Co1−Cl1 and Co1−Cl1^i 2.2361(13), N1−Co1−N1^i 100.6(2), Cl1−Co1−Cl1^i 127.14(9) [$i = -x, y, -z + \frac{1}{2}$].

Figure 3. Molecular structure of **3e**; thermal ellipsoids set at 35% probability (selected hydrogen atoms are omitted for clarity). Selected interatomic distances (Å) and angles (deg): Co1−N101 2.039(4), Co1−N201 2.059(4), Co1−Cl1 2.2350(16), Co1−Cl2 2.24131(16), N101−Co1−N201 105.95(16), Cl1−Co1−Cl2 114.02(6).
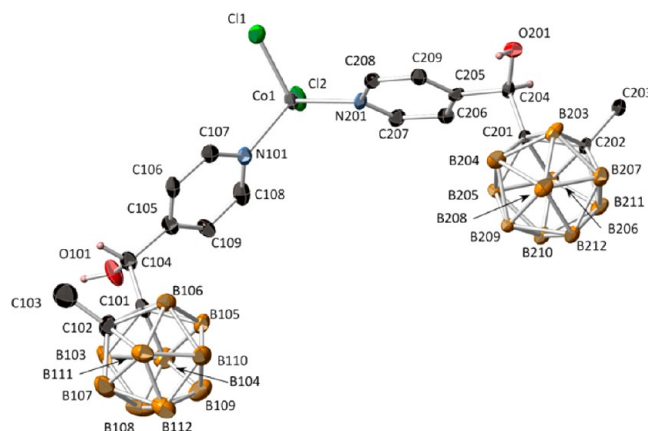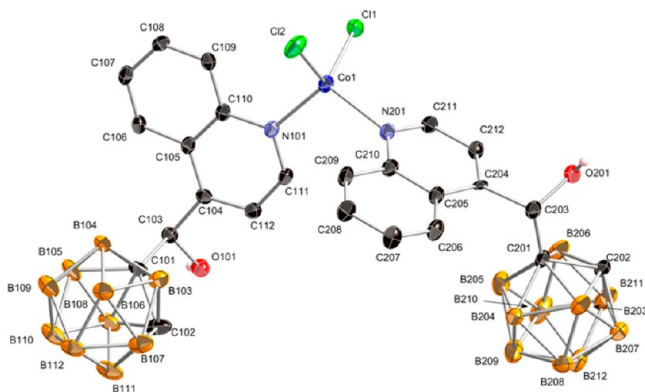

Figure 4. Molecular structure of **4c**; thermal ellipsoids set at 35% probability (1 of the 2 chemically identical independent molecules in the asymmetric unit; selected hydrogen atoms and ethanol solvent omitted for clarity). Selected interatomic distances (Å) and angles (deg): Co1−N101 2.025(5), Co1−N201 2.029(5), Co1−Cl1 2.255(2), Co1−Cl2 2.234(2), N101−Co1−N201 121.8(2), Cl1−Co1−Cl2 115.32(8).

angles show some interesting differences. Whereas the Co−N and Co−Cl bond lengths are very similar in both complexes (Figure 1), the Co−O bond lengths are significantly longer (0.031 Å) in the solvate complex **3a·2MeOH**. In addition, the N−Co−N angle in the latter complex is about 13° smaller than that in its solvate, and the O−Co−Cl angles are of the same order in both complexes. The latter differences are certainly the result of the hydrogen bonded methanol molecules in **3a·2MeOH**. The OH hydrogen atoms of both bidentate ligands in **3a·2MeOH** are interacting with the oxygen of a methanol molecule each, and this apparently weakens the Co−O bonds. This can be related with the behavior of complex **3a** in solution. Methanol solutions of **3a** are pink-violet and show a UV−vis spectrum consistent with an octahedral coordination (Figure 9). Interestingly, the latter pink-violet methanol solutions of **3a** turned blue on warming to about 70 °C, with the process being reversed on cooling (Figure 9). The spectroscopic shift from pink to blue when increasing the temperature is due to the shift of equilibrium from an octahedral to a
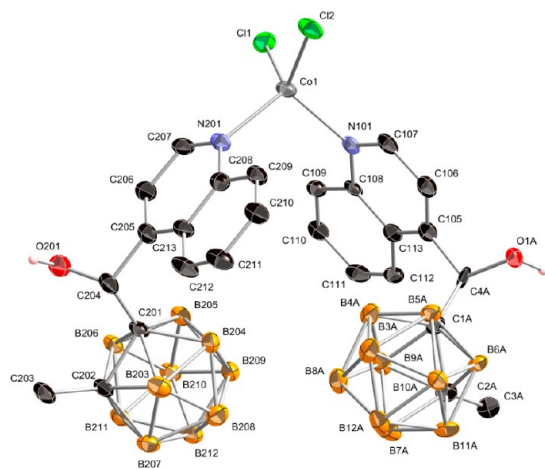
Figure 5. Molecular structure of **4e**; thermal ellipsoids set at 35% probability (disorder, and selected hydrogens omitted for clarity). Selected interatomic distances (Å) and angles (deg): Co1−N101 2.046(3), Co1−N201 2.047(3), Co1−Cl1 2.2352(14), Co1−Cl2 2.2403(13), N101−Co1−N201 99.68(13), Cl1−Co1−Cl2 108.92(5).
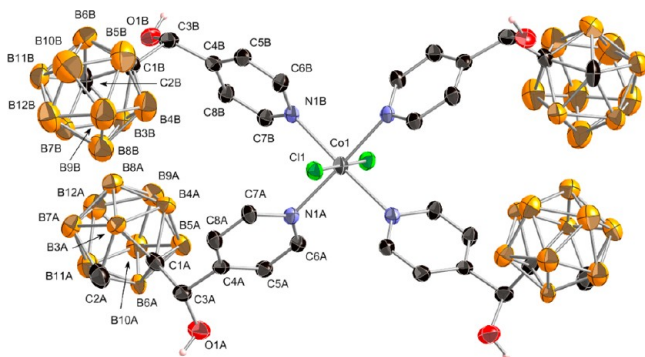

Figure 6. Molecular structure of **5**; thermal ellipsoids set at 35% probability (solvent and selected hydrogens omitted for clarity). Selected interatomic distances (Å) and angles (deg): Co1−N1A and Co1−N1A^i 2.173(7), Co1−N1B and Co1−N1B^i 2.155(7), Co1−Cl1 and Co1−Cl1^i 2.488(2), N1A−Co1−N1A^i 93.0(4), N1B−Co1−N1B^i 89.7(4), N1B−Co1−N1A and N1B^i−Co1−N1A^i 88.7(3), N1B−Co1−N1A^i and N1B^i−Co1−N1A 177.3(3), Cl1−Co1−Cl1^i 179.82(14) $[i = -x, y, -z + \frac{1}{2}]$.

Figure 7. Molecular structure of **6**; thermal ellipsoids set at 35% probability (selected hydrogens omitted for clarity). Selected interatomic distances (Å) and angles (deg): Co1−N1 and Co1−N1^i 1.975(2), Co1−O1 and Co1−O1^i 1.906(18), O1−Co1−N1 and O1^i−Co1−N1^i 84.19(9), O1^i−Co1−O1 180.00(8), and N1^i−Co1−N1 180.00(9) $[i = -x, -y, -z]$.

Figure 8. Molecular structure of **7**; thermal ellipsoids set at 35% probability (selected hydrogens omitted for clarity). Selected interatomic distances (Å) and angles (deg): Co3−N1 2.018(3), Co3−N2 1.952(3), Co3−O2 1.959(2), C3−O1 1.428(4), C9−O2 1.281(4), C9−O3 1.230(4), N1−Co3−N2 90.75(11), N1−Co3−O2 86.06(10), N2−Co3−O2 81.93(11).

tetrahedral structure.[18] This correlates with the weakening of the Co−O bonds observed in the crystal structure of **3a·2MeOH**. Thus, warming a methanol solution of **3a** seems to strengthen the O−H···O(methanol) hydrogen bond and consequently weaken the Co−O bonds, which eventually breaks to afford a tetrahedral coordinated complex in solution. This reasoning is further confirmed by dissolving **3a** in a better hydrogen bond acceptor solvent than methanol. Thus, acetone solutions of **3a** are blue at RT and give a characteristic spectrum for tetrahedral coordination (top of Figure 9). This experimental data shows, on one hand, the hemilabile character of the bidentate (2-pyridine)(*o*-carboranyl)methanol ligand in solution, but also tells us how to modulate, in principle, the Co−O bond of this ligand by solvent assisted intermolecular hydrogen bonding. This is certainly of interest for future catalytic and sensing applications of the present complexes in solution.

Supramolecular Structures. The supramolecular structures for complexes **3a**, **3a·2MeOH**, **3b**, **3e**, **4c**, and **4e** are dominated by nonconventional hydrogen bonds between the
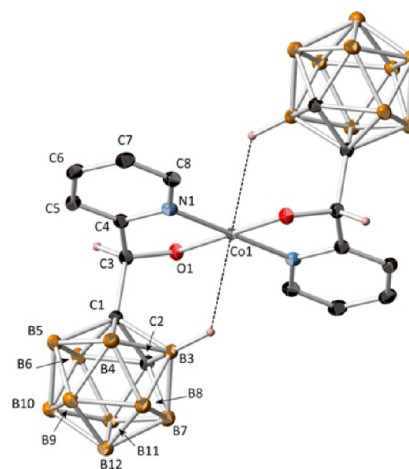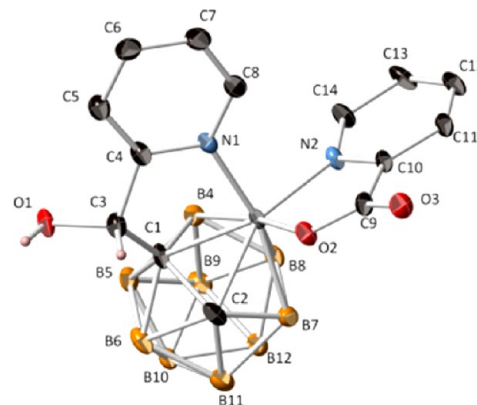
OH moiety of the *o*-carboranylalcohols and the chloride anions in the unsolvated structures or oxygen in the case of solvated ones (Figures 10 and 11). The distances of all of the observed intermolecular O−H···Cl/O hydrogen bonds are substantially shorter than the 2.95/2.72 Å distances, which corresponds to the sum of the van der Waals radii ($\sum$vdW) of hydrogen and chloride or oxygen atoms (Table 2) and is near-linear. Thus, they qualify as moderate hydrogen bonds.[19] In addition, $\pi-\pi$ interactions through the N-aromatic rings are observed in most of the structures, as shown in Figure 11 and Table 3. In order to better understand the supramolecular structures for these complexes, we will divide the compounds into two groups: Group A—those where *o*-carboranylalcohol-pyridines act as N,OH chelating ligands and therefore the hydroxyl group is coordinated to the metal (Scheme 3 and Figure 1)—Group B—those where *o*-carboranylalcohol-pyridines act as monodentate N donor ligands and consequently the hydroxyl group is uncoordinated (Scheme 3 and Figures 2−6). In addition, we

Table 1. Crystallographic Parameters for Complexes 3a, 3a·2MeOH, 3b, 3e, 4c, 4e, 5, 6, and 7[a]

	3a	3a·2MeOH	3b	3e	4c	4e	5	6	7
empirical formula	$C_{16}H_{34}B_{20}Cl_2CoN_2O_2$	$C_{18}H_{42}B_{20}Cl_2CoN_2O_4$	$C_{16}H_{34}B_{20}Cl_2CoN_2O_2$	$C_{36}H_{62}B_{20}Cl_2CoN_2O_6$	$C_{20}H_{44}B_{20}Cl_2CoN_2O_3$	$C_{26}H_{42}B_{20}Cl_2CoN_2O_2$	$C_{36}H_{80}B_{40}Cl_2CoN_4O_6$	$C_{16}H_{32}B_{20}CoN_2O_2$	$C_{14}H_{30}B_9CoN_2O_3$
formula weight	632.48	696.57	632.48	964.91	706.60	760.65	1227.27	559.57	420.54
crystal system	orthorhombic	orthorhombic	monoclinic	monoclinic	orthorhombic	triclinic	monoclinic	monoclinic	triclinic
space group	Pcca	Pccn	C2/c	P2₁/c	Pna2₁	P1̄	C2/c	P2₁/c	P1̄
a (Å)	21.5590(10)	18.545(4)	21.4535(6)	17.5338(7)	14.4006(3)	11.7395(4)	31.2140(16)	10.9367(2)	9.357(5)
b (Å)	13.4149(7)	13.040(3)	12.1851(3)	28.8699(13)	22.0313(5)	12.3117(4)	15.6420(7)	10.1603(2)	9.914(5)
c (Å)	11.4446(4)	14.563(3)	12.9133(4)	10.3153(5)	23.8677(5)	14.8750(5)	13.5450(6)	13.3471(3)	10.463(5)
α (deg)						76.758(2)			96.530(7)
β (deg)			112.7260(14)	101.8810(10)		76.878(2)	93.772(2)	111.1610(10)	94.002(7)
						64.632(2)			103.836(7)
volume (Å³)	3309.9(3)	3521.8(12)	3113.62(15)	5109.7(4)	7572.4(3)	1870.56(11)	6599.0(5)	1383.12(5)	931.6(8)
Z	4	4	4	4	8	2	4	2	2
ρ_{calcd} (g cm⁻³)	1.269	1.314	1.349	1.254	1.240	1.350	1.235	1.344	1.499
abs coeff (mm⁻¹)	0.702	0.670	0.746	0.484	0.623	0.634	0.386	0.644	0.940
F(000)	1284	1428	1284	2004	2904	778	2532	570	428
crystal	lath; pale purple	rod; violet	fragment; dark blue	fragment; blue	block; blue	fragment; intense blue	plate; colorless	fragment; colorless	oval; violet
crystal size (mm)	0.18 × 0.06 × 0.02	0.18 × 0.10 × 0.08	0.20 × 0.09 × 0.03	0.12 × 0.08 × 0.04	0.12 × 0.10 × 0.08	0.17 × 0.10 × 0.05	0.20 × 0.20 × 0.03	0.11 × 0.052 × 0.03	0.20 × 0.20 × 0.18
θ range for data colletn (deg)	3.01–25.03	3.01–27.48	3.24–27.48	2.92–25.02	2.95–25.03	3.04–25.03	3.01–25.03	3.16–27.48	3.09–27.48
reflns colletd	2902	20666	18875	38693	11876	284012	52539	14856	8895
ind reflin	2902	4030	3550	8984	11876	6582	5830	3160	4226
		[R_{int} = 0.0339]	[R_{int} = 0.0632]	[R_{int} = 0.0612]		[R_{int} = 0.0734]	[R_{int} = 0.2416]	[R_{int} = 0.0560]	[R_{int} = 0.0306]
completeness to θ = (deg), (%)	25.03, 99.4	27.48, 99.8	27.48, 99.7	25.02, 99.6	25.03, 99.7	25.03, 99.6	25.03, 99.8	27.84, 99.6	27.48, 98.9
max. and min. transmission	0.9861 and 0.8841	0.9483 and 0.8889	0.9780 and 0.8651	0.9809 and 0.9442	0.9519 and 0.9290	0.9690 and 0.8999	0.9885 and 0.9268	0.9810 and 0.9326	0.8490 and 0.8342
largest diff peak and hole (e Å⁻³)	0.648 and −0.373	0.300 and −0.309	2.710 and −0.569	1.373 and −0.763	0.614 and −0.574	1.288 and −1.025	1.528 and −0.516	0.470 and −0.383	1.388 and −0.437
data/restraints/parameters	2902/0/199	4030/0/222	3550/72/196	8984/132/612	11876/522/873	6582/208/528	5830/120/407	3160/0/187	4226/0/266
goodness-of-fit on F²	1.178	1.170	1.080	1.129	1.056	1.018	1.477	1.094	1.086
final R indices [F² > 2σ(F²)]	R1 = 0.0654 wR2 = 0.1413	R1 = 0.0456 wR2 = 0.0960	R1 = 0.0878 wR2 = 0.2010	R1 = 0.0959 wR2 = 0.1866	R1 = 0.0736 wR2 = 0.1677	R1 = 0.0787, wR2 = 0.1586	R1 = 0.1357, wR2 = 0.3308	R1 = 0.0544, wR2 = 0.1041	R1 = 0.0554, wR2 = 0.1246
R indices (all data)	R1 = 0.0819 wR2 = 0.1479	R1 = 0.0483 wR2 = 0.0973	R1 = 0.1166 wR2 = 0.2217	R1 = 0.1161 wR2 = 0.1976	R1 = 0.0991 wR2 = 0.1812	R1 = 0.1147, wR2 = 0.1814	R1 = 0.1950, wR2 = 0.3520	R1 = 0.0718, wR2 = 0.1132	R1 = 0.0628, wR2 = 0.1282

[a]CCDC 828992 (3a), 884178 (3a·2MeOH), 828991 (3b), 884179 (3e), 884180 (4c), 884181 (4e), 884282 (5), 884183 (6), and 884184 (7) contain the supplementary crystallographic data for this paper. These data can be obtained free of charge from The Cambridge Crystallographic Data Centre via www.ccdc.cam.ac.uk/data_request/cif.
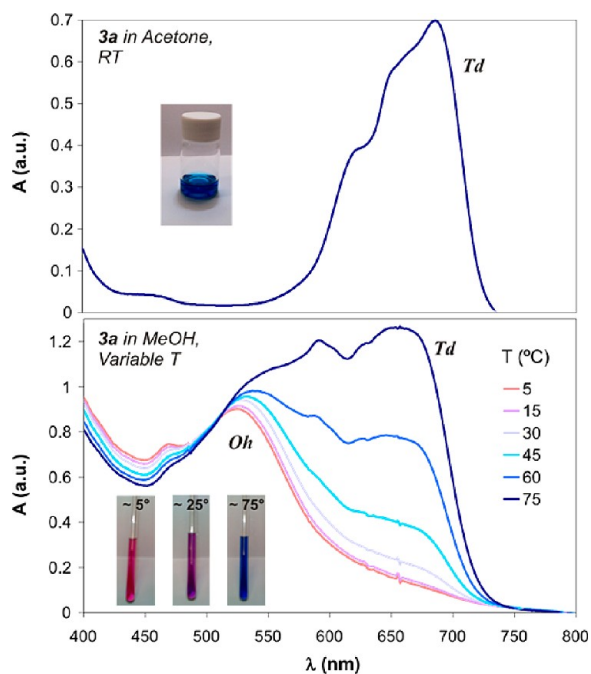
Figure 9. (top) UV–visible spectrum of **3a** in acetone at RT. (bottom) Spectroscopic evidence of the temperature dependence equilibrium for **3a** in methanol (5–75°).

will compare the supramolecular structures in Group A with those of related complexes.

Group A: Structures with Chelating N,OH Ligands. Complex **3a** forms chains, alternating *RR* and *SS* enantiomeric complexes, along the *c* axis via O—H···Cl hydrogen bond interactions (Figure 10 and Table 2). In **3a** the hydroxyl donors are coordinated to the metal, resulting in a tight $R_2^2(8)$ ring.[2] Very interestingly, the methanol solvate of the latter, **3a·2MeOH**, also shows chains of alternating *RR* and *SS* enantiomeric complexes. However, two methanol molecules are inserted now in the hydrogen bonding network, resulting in a more open R4,4(12) ring (Figure 10, bottom). Thus, in **3a·2MeOH** each coordinated hydroxyl donor interacts with the oxygen atom of a methanol molecule (O—H···O(H)Me) and the hydroxyl hydrogen atoms of the latter act as donors and form hydrogen bonds with the chlorides of another complex (MeO—H···Cl), as shown at the bottom of Figure 10. The arrangement of molecules along the chains (right column of Figure 10) shows how carborane cages of consecutive molecules are staggered in **3a** but are eclipsed in **3a·2MeOH**. The three-dimensional (3D) structures of **3a** and **3a·2MeOH** are built by self-assembly of the polymeric hydrogen bonded networks shown in Figure 10, which are dominated by weak dihydrogen and/or hydrophobic interactions. Another interesting feature of the supramolecular structure of **3a** is that it contains one-dimensional channels (the crystal structure showed some residual electron density in these
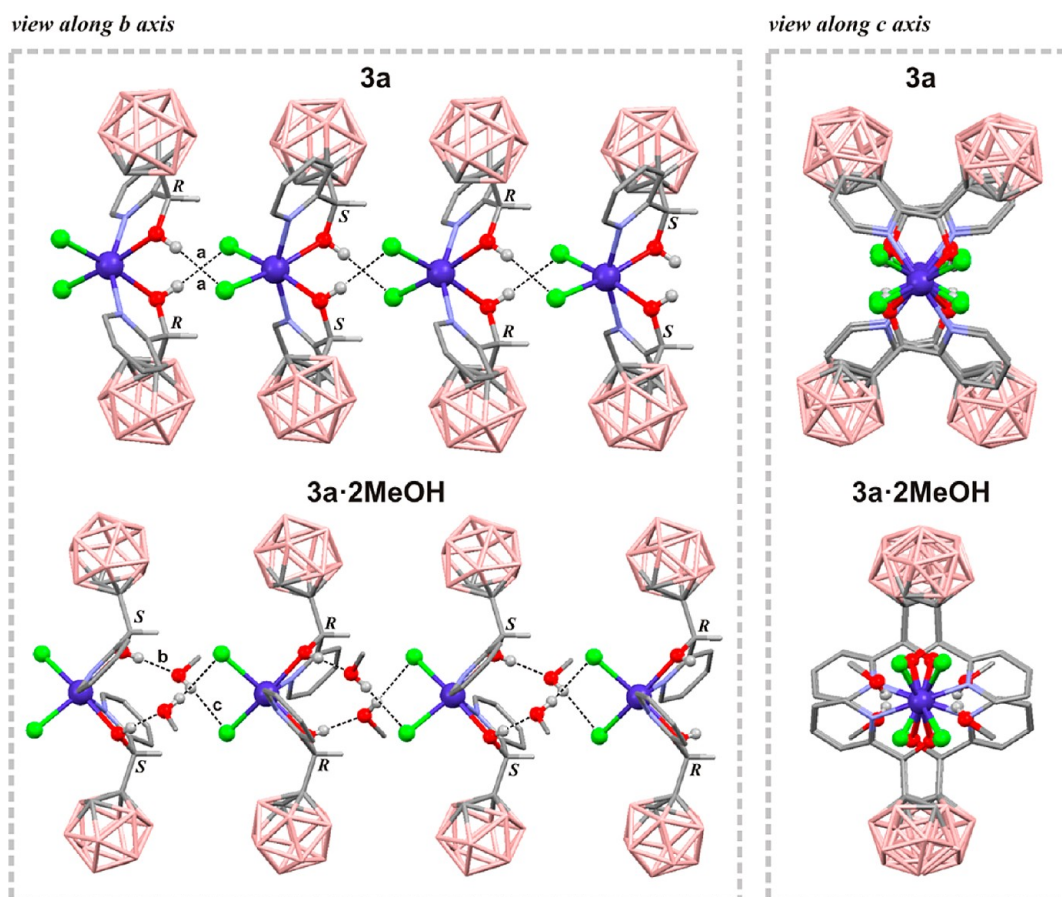

Figure 10. Supramolecular assemblies of **3a** and **3a·2MeOH**. Left column: Projections showing four molecules of each compound forming hydrogen bonded chains. Right column: Projections along the hydrogen bonded chains showing a staggered arrangement of the carboranyl fragments in **3a** (top) versus an eclipsed arrangement in **3a·2MeOH** (bottom). See Table 2 for metric parameters. All hydrogen atoms, except those for the CHOH group, are omitted for clarity. Color code: B, pink; C, gray; H, white; O, red; N, light blue; Cl, green; Co, blue.

Figure 11. Supramolecular assemblies of **3b**, **3e**, and **4e**. Projections showing four molecules for each compound. Dashed red lines indicates π−π interactions. For complex **3e** only hydrogen bonded acetone molecules are shown (Supporting Information). See Tables 2 and S1 for metric parameters. All hydrogen atoms, except those for the CHOH group, are omitted for clarity. Color code: B, pink; C, gray; H, white; O, red; N, light blue; Cl, green; Co, blue.
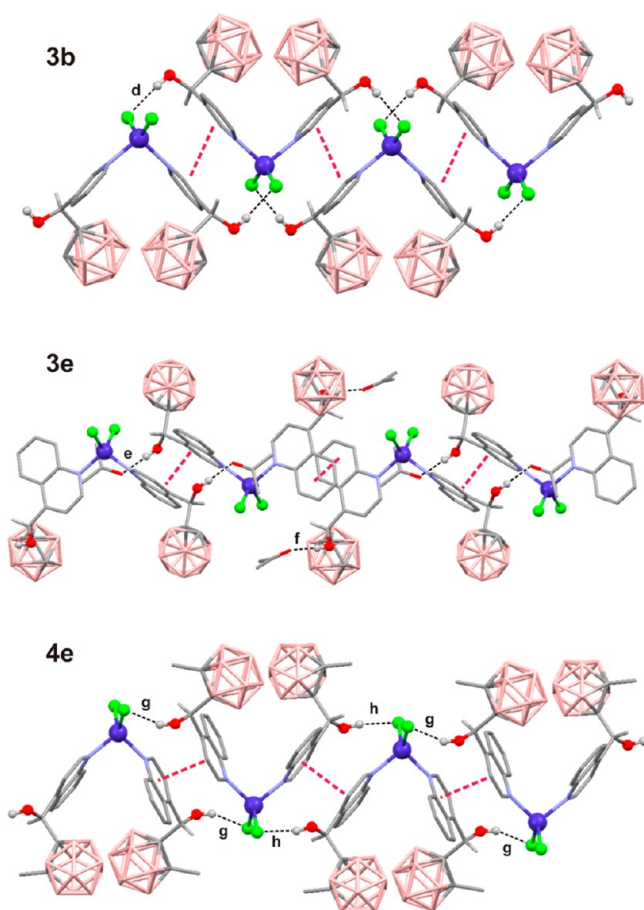
channels) running along the *c* axis parallel to hydrogen bonded chains (Figure 12). The consequences of the supramolecular structures of **3a** and **3a·2MeOH** will be described below.

Group B: Structures with Monodentate N,OH Ligands. The supramolecular structures for the unsolvated complexes **3b** and **4e** show both chains via O−H···Cl interactions, where *RR*

and *SS* enantiomeric complexes alternate (Figure 11), as already observed for complex **3a**. However, unlike the case of **3a**, in **3b** and **4e** the hydroxyl donor is uncoordinated, allowing the formation of more open $R_2^2(16)$ and $R_2^2(18)$ rings,[2] respectively, which gives place to additional π−π interactions through the pyridine or quinoline rings of adjacent molecules (Figure 11 and Table 3).

Regarding the supramolecular structures of **4c**, **3e**, and **5**, all contain oxy-solvents (either ethanol or acetone). The supramolecular structure for complex **4c** will not be considered due to poor data. In all cases, the solvent interferes in the expected O−H···Cl hydrogen bonding chains (*vide supra*). Thus, each molecule in the solid structure of **3e** forms two O−H···O=CMe₂ hydrogen bonds with acetone as the acceptor (middle of Figure 11). But even in the absence of a polymeric hydrogen bonding network, the molecules in **3e** are self-assembled by intermolecular π−π interactions through the quinoline rings of adjacent molecules. The latter supramolecular arrangement is similar to that found in **4e**, as shown in Figure 11 (bottom). It is also noteworthy that, in the absence of such a hydrogen

Table 3. N-Aromatic−N-Aromatic Ring Packing Geometries (Å, deg), Involved in the Supramolecular Construction in 3b, 3e, 4e, and 5[a]

M = Centroid

compd	interplanar distance	interplanar angle	d^b	Hd^c	$θ^d$
3b	3.471	0.00	3.875	1.723	26.4
3e	3.605	0.00	3.705^e	0.852	13.3
4e	3.410	0.00	3.698^f	1.951	31.9
	3.428	0.00	3.677^g	1.330	21.2
5	4.269	0.00	4.959	2.524	30.6

[a]See embedded chart at the top for nomenclature. [b]Ring centroid to ring centroid distance. [c]Horizontal displacement between the two ring centroids. [d]Ring normal to vector between the ring centroids angle. [e]Distance between carbon rings of quinolyl fragments (C205−C210). [f]Distance between carbon and pyridine ring fragments in quinolyl (C208−C213 and C205C206C207N201C208C213). [g]Distance between carbon and pyridine ring fragments in quinolyl rings (C108−C113 and C105C106C1207N101C108C113).

Table 2. Geometrical Parameters of Intermolecular O−H···A (A = O, Cl) Contacts (Å, deg), Involved in the Supramolecular Construction in 3a, 3a·MeOH, 3b, 3e, 4e, and 5

compd	O−H···A^a	d(H···A)	d(O···A)	∠(OHA)
3a	(a) O(1)−H···Cl(1)^i	2.28(6)	3.121(3)	173(5)
3a·2MeOH	(b) O(1)−H···O(2)^{ii}	1.84(3)	2.581(2)	176(3)
	(c) O(2)−H···Cl(1)	2.40(3)	3.1887(17)	168(3)
3b	(d) O(1)−H···Cl(1)^{iii}	2.225(1)	3.059(5)	171.6(4)
3e	(e) O(101)−H···O(301)^{iv}	1.866(4)	2.704(5)	175.8(3)
	(f) O(201)−H···O(401)	1.819(5)	2.657(6)	176.0(3)
4e	(g) O(1A)−H···Cl(1)^v	2.316(1)	3.097(4)	155.1(3)
	(h) O(201)−H···Cl(2)^{vi}	2.285(1)	3.064(3)	154.5(2)
5	(i) O(1A)−H···O(101)^{vii}	1.825(6)	2.636(10)	162.1(5)
	(j) O(1B)−H···Cl(1)^{viii}	2.208(2)	3.031(7)	166.7(5)

^{a}O−H bond lengths not normalized to neutron distances. See interactions a−j in Figures 10 and11. Symmetry codes: (i) *x*, −*y* + 1, *z* − ¹/₂; (ii) −*x* + ³/₂, *y*, z − e; (iii) −*x* + 1, −*y*, −*z*; (iv) −*x*, −*y*, −*z*; (v) −*x*, −*y* + 1, −*z*; (vi) −*x*, −*y* + 1, −*z* + 1; (vii) −*x*, *y*, −*z* + ³/₂; (viii) *x*, −*y*, *z* + ¹/₂.
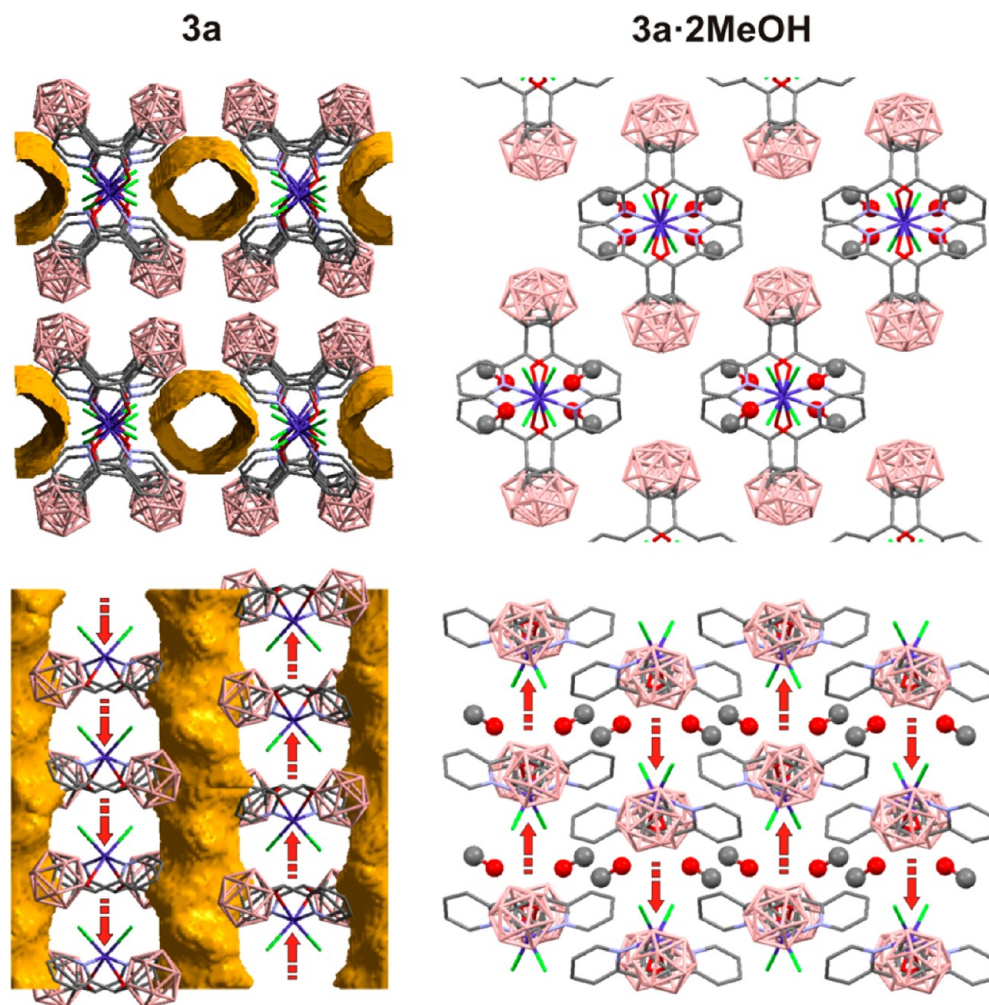
Figure 12. Comparison of the 3D supramolecular assemblies of **3a** (left) and **3a·2MeOH** (right) showing the well-defined channels (yellow-orange) running along the *c* axis in the former and the absence of voids in the latter. The figure shows comparative views along the hydrogen bonded chains (top) and perpendicular to the chains (bottom; dashed red arrows indicate the propagation direction of the hydrogen bonds). Methanol molecules are shown in ball and stick style. Color code: B, pink; C, gray; O, red; N, light blue; Cl, green; Co, blue.

bonding network, molecules segregate as *SR* enantiomeric complexes. Another interesting feature of **3e** is that, apart from the interacting acetone molecules mentioned above, it contains disordered solvent molecules (also acetone) in voids along the crystallographic *c* axis (Figure S41 of the Supporting Information). The crystal structure of **5** contains two molecules of ethanol per each complex. Thus, half of the OH moieties in each complex are involved in intermolecular O—H···Cl and the other half in O—H···Cl hydrogen bonds (Figure S40 and Table 2). Additional weak π−π interactions through the pyridine rings of adjacent molecules are also observed in **5** (Table 3).
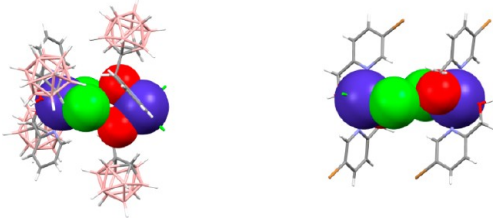
Comparison of Structures. It is instructive to compare the supramolecular structures for all complexes in order to understand the supramolecular consequences of molecular changes. The packing arrangement of molecules in a molecular crystal is governed by the interplay of the tendency to close packing and the strength of the intermolecular interactions. As already described above, all new compounds show intermolecular O—H···Cl/O hydrogen bonds. From those, unsolvated structures show exclusively O—H···Cl hydrogen bonds giving supramolecular chains (**3a**, **3b**, and **4e**). The latter chains are interrupted whenever an oxygen containing solvent is included

in the structures. In this situation, O—H···O hydrogen bonds are also formed, interfering partially (**5**) or totally (**3e**) into the O—H···Cl hydrogen bonds. In addition to the above hydrogen bonding scheme, those complexes where the hydroxyl group is not coordinated to the metal, additional π−π interactions through the N-aromatic rings are observed (Table 3). The interplanar distances in compounds **3b**, **3e**, and **4e** are within the limits observed for common π-stacked aromatic rings.[20] The ring normal and the vector between the ring centroids and the centroid−centroid distances between N-aromatic rings show that the supramolecular structures of **3b**, **3e**, and **4e** consist of closely packed parallel slightly offset aromatic ring π−π interactions (Table 3). The offset is larger in the case of **5** due to the bulkiness of this complex. It is also highly instructive to compare the supramolecular structures of the tetrahedral coordinated complexes **3b**, **3e**, and **4e** (Figure 11), as all show very similar supramolecular arrangements. Whereas the arrangements of molecules in **3b** and **4e** are sustained by O—H···Cl hydrogen bonds and π−π interactions, that for **3e** is due, exclusively, to π−π interactions as the acetone included interferes in the hydrogen bonds that would otherwise probably be formed with Cl atoms. Thus, molecules seem to pack so as

to optimize $\pi-\pi$ interactions between aromatic rings. This simply suggests that both hydrogen bonds and $\pi-\pi$ interactions compete to give the observed supramolecular structures and can be considered structure directing interactions in the case of tetrahedral cobalt complexes of the carboranyl alcohol ligands. This is further supported by the relative strength of hydrogen bonding versus $\pi-\pi$ interactions in 3b and 4e. Whereas the O—H···Cl hydrogen bonds are stronger in the pyridine derivative 3b (Table 2), the $\pi-\pi$ interactions are stronger in the case of the quinoline derivative 4e (Table 3). It is well-known that larger aromatic systems favor the $\pi-\pi$ interactions.[21] So in complex 4e the intermolecular $\pi-\pi$ interactions are optimized against the O—H···Cl hydrogen bonds. This is confirmed when looking at the supramolecular structure for 3e (Figure 11). In this case, O—H···O hydrogen bonds—not giving polymeric networks—are exclusively formed with acetone molecules. But even so, the molecules arrange in a similar way to those in 4e and are exclusively sustained by $\pi-\pi$ interactions. The interplanar distance between the quinoline rings in 4e is about 0.2 Å shorter than that in 3e.

Regarding the octahedral complex 3a, the arrangement of molecules in each hydrogen bonded chain pushes the four non-hydrogen atoms of the interaction (2O and 2Cl) into a hexagonal close packing-like arrangement forming a tetrahedron (D···A···A···D torsion = −62.09°) as shown in Table 4. In

Table 4. Different Spatial Arrangement of Oxygen and Chloride Atoms as a Consequence of the Hydrogen Bonding Networks Observed in 3a, 3a·2MeOH, and Related Complexes[a]


compd	$d(O\cdots Cl)$	O···Cl···Cl···O torsion	Co···Co
3a	3.121(3)	−69.09	5.722
3a·2MeOH	3.1887(17)	+30.54	7.281
8	3.048	0.0	6.129
9	3.068	0.95	6.254

[a]See embedded supramolecular assemblies for two molecules of 3a (left) and 8 (right) with Co, O, and Cl atoms in space fill style. Color code: B, pink; C, gray; H, white; O, red; N, light blue; Cl, green; Co, blue. Distances and angles in Å and deg.

comparison, the arrangement of molecules in the chains in 3a·2MeOH involves a more square planar arrangement (D···A···D···A torsion = −30.54°) due to the larger separation between molecules as a consequence of the insertion of methanol into the hydrogen bonding network. Thus, whereas the Co···Co separation in 3a is 5.722 Å, that for the methanol solvate 3a·2MeOH is 7.281 Å. As mentioned above, the arrangement of molecules along the hydrogen bonded chains in the complexes shows how the carborane cages of consecutive molecules are staggered in 3a (Figure 10, top right) but eclipsed in 3a·2MeOH (Figure 10, bottom right). This has important consequences in the three-dimensional (3D) structures of these two complexes as shown in Figure 12. The 3D structures of 3a and 3a·2MeOH are built by self-assembly of the polymeric hydrogen bonded chains (staggered for 3a and

eclipsed for 3a·2MeOH). As can be seen in Figure 12, the eclipsed chains in 3a·2MeOH are better closed packed than the staggered chains in 3a. The packing of the latter chains creates defined channels running along the c axis parallel to hydrogen bonded chains (Figure 12). Complex 3a is therefore an extrinsic porous molecular complex.[22]

Scheme 5. Different Arrangements of Donors (D = OH) and Acceptors (A = Cl) within Adjacent Molecules (squares)[a]
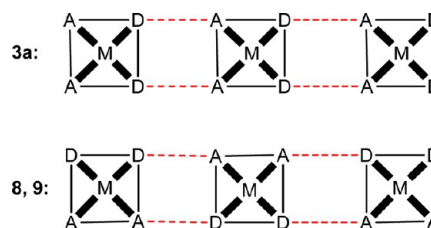
[a]Dashed red lines represent hydrogen bonds. M = metal.

A comparison of the molecular and supramolecular structures of the octahedral complex 3a with those of related cis-CoCl₂(L)₂ (L = 5-Br-hmpH (8)[14c] or 2-(1-aziridinyl)ethanol-(9)[14d] complexes highlights some interesting features. The structural core for these complexes and that for 3a are basically identical: the hydroxyl group is coordinated to the metal, and their supramolecular structures are all based on intermolecular O—H···Cl hydrogen bonds (Supporting Information). In complexes 8 and 9, the arrangement of molecules in the hydrogen bonded chains involves a more square planar arrangement (D···A···D···A torsion = 0.0° and 0.95°) than in 3a which minimizes the D···A distances at the expense of the Co···Co separation, as shown in Table 4. In addition to that, the arrangements of the hydrogen bonds in 8 and 9 present some notable differences with that for 3a. In the latter complex, both hydroxyls are located on the same side (with respect to the propagation direction of the chain), resulting in a double donor interaction (Figure 10 and Scheme 5) while in 8 and 9 each molecule presents both a hydroxyl and a chlorine to the adjacent molecule, forming a mixed donor/acceptor interaction along the chain as shown in Scheme 5 and the Supporting Information.

Another major difference between our complexes and 8 and 9 is that our carboranyl ligands are chiral. As mentioned above, the supramolecular structures for those of our complexes that show intermolecular O—H···Cl hydrogen bonding networks (3a, 3a·MeOH, 3b, and 4e) are that the complexes form chains, alternating RR and SS enantiomeric complexes. Interestingly, we are aware of only one other hydrogen bonding network of the type found in 3a, and that corresponds to the Mn complex cis-MnCl(C₅H₁₀O₂)₂ (10), having also two chiral bidentate ligands per metal;[23] however, in this case the enantiomers are segregated into separate chains. So it appears that the chirality in conjunction with the bulky carborane favors RR/SS alternation as a more economic packing arrangement. Unlike 3a, those related complexes not having the carboranyl fragment in their molecular structures do not present solvent accessible pores in their structures.

Magnetic Properties. As a representative study and with the aim of investigating the possible relationship between supramolecular structure and physical properties, solid-state, variable-temperature (2−300 K) magnetic susceptibility data were collected on polycrystalline samples of the three pyridyl based carboranylalcohol complexes 3a−c with applied fields of 0.03

and 1.0 T for compound **3a** and 0.05 T for **3b** and **3c**. The resulting data for all three compounds are plotted by means of $\chi_M T$ vs T in Figure 13. The magnetic moment of 4.83 μB, 4.38 μB, and
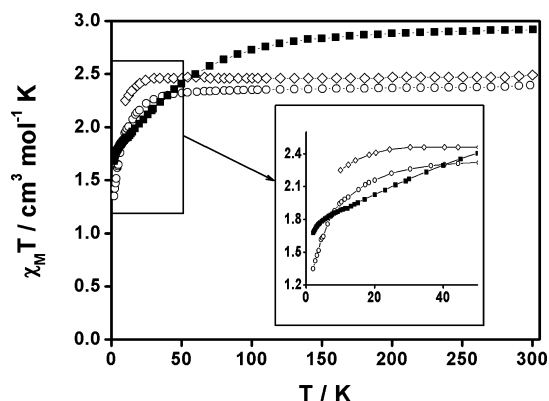

Figure 13. $\chi_M T$ vs T plots for compounds **3a** (black squares), **3b** (white circles), and **3c** (white rhombs) between 2.0 and 300.0 K. Inset: Increased section of the graph containing all three compounds from 2 to 50 K. Solid lines in $\chi_M T$ vs T plots are guides for the eye.

4.46 μB observed at room temperature for **3a**, **3b**, and **3c** respectively, is in agreement with the reported range for Co[II] complexes, which takes into account the orbital magnetic momentum (4.7−5.2 μB for octahedral and about 4.59 μB for tetrahedral ones) and lies higher than that expected for a magnetically isolated $S = \frac{3}{2}$ system (3.87 μB assuming $g = 2.0$).[24]

For **3a**, the product of the magnetic susceptibility and temperature smoothly decreases upon cooling until approximately 100 K (because of the spin−orbit effect) and then drops faster, reaching a value of 1.68 cm³ mol⁻¹ K at 2 K (Figure 13 inset). The M/Nμ_B vs H curve is also included in the Supporting Information (Figure S18). The data above 20 K obeys the Curie−Weiss law with $C = 3.04$ cm³ mol⁻¹ K and $\theta = -11.83$ (C and θ, Curie constant and temperature, respectively; Figure S19). On the other hand, compounds **3b** and **3c** show similar behaviors; their magnetic susceptibility data are mostly constant until 30 K and drop dramatically to 1.35 and 2.25 cm³ mol⁻¹ K at 2 and 10 K, respectively. Likewise, for compound **3a**, the Curie−Weiss law provides values of $C = 2.40$ and 2.48 cm³ mol⁻¹ K and $\theta = -1.95$ and -0.59 for **3b** and **3c**, in that order (Figure S45). The negative sign of θ can be related with the weak but significant antiferromagnetic couplings among the monomeric units, and in the case of compounds **3a** and **3b**, whose crystalline structure is known, it is possible to associate this with the number of observed hydrogen bonds that provide the through space exchange (Figure 10). The arrangements in the crystal packing of **3a** and **3b** account for the different observed values for θ; in the first case, the 2-pyridine chelating ligands give rise to supramolecular 1D chains where the metal centers are perfectly aligned and separated only by the Cl···H−O moieties, suggesting stronger interaction than that obtained by experiment for the second one, where the o-carboranylalcohol 3-pyridine is located between the Co[II]. Related to such observation, a modest sigmoidal shape is observed for the $\chi_M T$ data below 30 K of **3a** (Figure 13, inset). In the absence of crystallographic data for **3c**, the small θ value suggests that the interactions between units for this complex are comparable to those appearing in **3b**.

Porosity and Structural Transformations in Complex 3a. Porous materials have found widespread applications in a range of areas for many years[25] and have become some of the most technologically relevant systems across materials chemistry. More recently, a huge range of such chemical systems have been under investigation for gas storage.[26] As previously mentioned, there are many such materials which self-assemble around solvent-containing cavities to form solid state structures. In such a case, the initial criterion for a potentially useful system will be the robustness of the molecular architecture to the removal of solvent, and the consequent preservation of the cavity of potential value for application to gas storage. In that sense, complex **3a** could be considered a good candidate. As discussed before, when crystals of **3a** are grown from ethanol or acetone, they adopt a porous structure with channels running along the crystallographic c-axis containing disordered solvent (Figure 12). To investigate the possibility of extracting the solvent from the pores, crystals from **3a** obtained from acetone were dried under vacuum at different temperatures. Elemental analysis of crystals of **3a**, dried under vacuum at RT, already confirmed the absence of solvent. Powder X-ray diffraction (PXRD) analysis of the unsolvated crystals showed a powder pattern that matched the calculated one from the X-ray structure (Supporting Information). Further heating of the crystals at 90 °C for several hours did not affect the powder pattern. DSC and TGA measurements corroborated the absence of solvent in a crystalline sample of **3a** dried under vacuum at RT (red lines in Figure 14). TGA scans of the unsolvated crystals
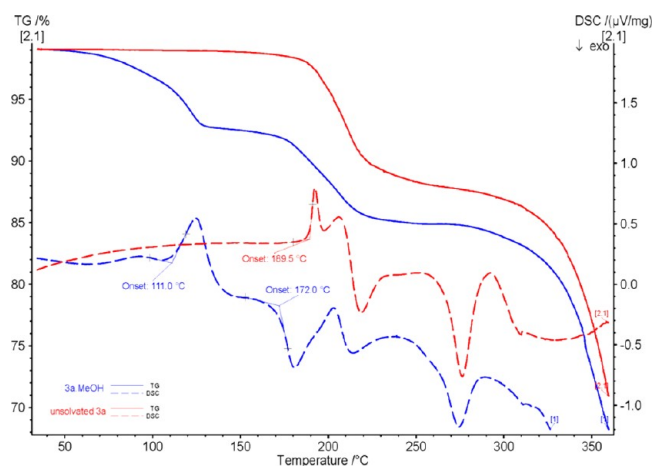

Figure 14. Partial TGA (continuous lines) and DSC (dashed lines) plots for **3a** after drying under vacuum (red) and after being exposed to methanol vapor (blue).

for **3a** did not show any weight loss prior to melting and decomposition. TGA of **3a** shows that the complex is stable up to 190 °C, and decomposition starts at this temperature and takes place in two steps (190−266 °C, 10.59% mass loss; 290−430 °C, 35.46% mass loss). All these data confirm that the solvent can be extracted from the pores of **3a** by simply drying the material at RT and that the structure and crystallinity are maintained after extraction. Consequently, these experiments demonstrate that the porous structure in **3a** is not a solvent-templated process, and as mentioned, one promising utility lies in its potential for gas storage. Complex **3a** is certainly a rare example of a porous carborane-based metal−organic molecular material where molecules are, in contrast to porous carborane-based metal−organic frameworks,[27] interacting by noncovalent interactions. Gas sorption experiments will be carried out and the results reported in a future paper.

As mentioned above, if the crystallization of **3a** is performed in methanol, the solvent is incorporated in the structure intercepting the O−H···Cl intermolecular interactions shown in the porous crystal and resulting in the solvate **3a·MeOH** (Figures 10 and 12). As previously discussed, the different arrangement of the carboranyl fragments in the supramolecular structures for these two complexes explains the presence or absence of voids. These two different structures account for the dynamism of this molecular system and, thus, encouraged us to study the possibility of solvent mediated transformation in the solid state. The capability of **3a** to uptake solvent vapors to convert into **3a·2MeOH** has been demonstrated experimentally (Figure 15). The identity of the products was confirmed by
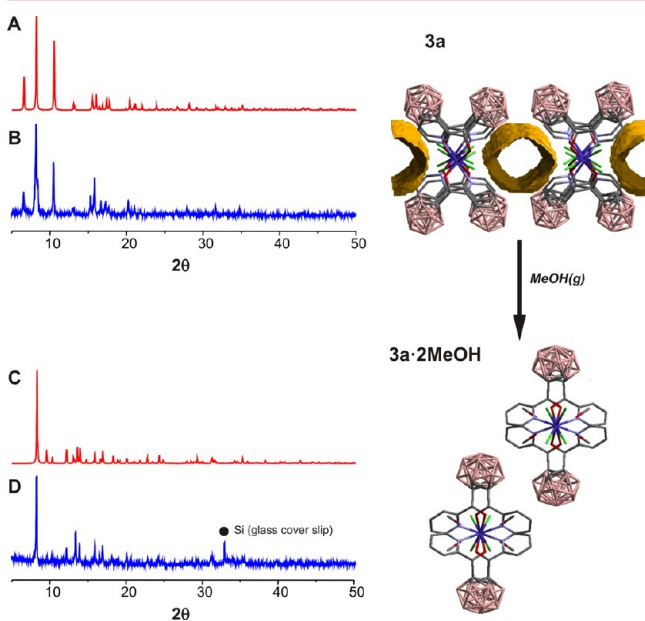

Figure 15. Solid state transformation of **3a** into **3a·2MeOH**. Left: Comparison between calculated and experimental PXRD patterns (A and B) for unsolvated powder of **3a** and (C and D) after solvation experiments. Right: Scheme for the solid transformation according to the PXRD.

X-ray powder diffraction, which matched the calculated diffraction patterns from the single crystal X-ray structures. Freshly made dried violet powder for **3a** gives a powder diffraction pattern that closely matches the one simulated from the single-crystal data, thereby proving that a homogeneous and single-crystalline phase has resulted during synthesis (top of Figure15). The powder sample for **3a** converts to the solvate **3a·2MeOH** when left in contact with methanol vapors for a week (bottom of Figure 15). TGA of **3a·2MeOH** shows release of methanol guest molecules between 100 and 140 °C before decomposition (blue line in Figure 14). DSC measurements show an endothermic peak at 111 °C for the desolvation process in **3a·2MeOH**, followed by a broad exothermic peak at 172 °C, and then the thermal events behave identically to those for **3a**. The exothermic peak observed in **3a·2MeOH** is consistent with molecular shrinkage within the supramolecular chains with formation of new hydrogen bonds due to release of hydrogen bonded methanol and formation of **3a**. However, the solvation process proved to be irreversible, since powder **3a·2MeOH** did not lose methanol by heating under vacuum at 90 °C and further heating until 150 °C caused partial

decomposition and the formation of an amorphous material. Thus, although irreversible, the solvation process is remarkable, since the unsolvated compound is related to the methanol solvated compound by rotation of complex molecules within the 1D O−H···Cl hydrogen bonding networks and insertion of methanol into the network. This could be explained by diffusion of methanol vapors into the empty channels in **3a**, followed by interaction of the solvent with the O−H···Cl hydrogen bonding network and consequential insertion of methanol into the network −therefore cleavage of O−H···Cl and formation of O−H···O(Me)−H···Cl hydrogen bonds—causing a separation and rotation between molecules to afford **3a·2MeOH**.

■ CONCLUDING REMARKS

In conclusion, we present here the first family of metal complexes CoCl$_2$(LOH)$_2$ (**3a−c** and **4a−c**) with the recently reported series of *o*-carboranylalcohols bearing pyridines or quinolines as ligands (LOH: 1-[R(hydroxy)methyl]-2-R′-1,2-dicarba-*closo*-dodecaborane (R′ = H or Me; R = 2-pyridyl **1a** or **2a**, 3-pyridyl **1b** or **2b**, 4-pyridyl **1c** or **2c**, 2-quinolyl **1d** or **2d**, 4-quinolyl **1e** or **2e**)). As expected from the colors of the complexes, the molecular structures for the 2-substituted ligands (**3a**, **4a**) and 3- and 4-substituted ones (**3b−c**, **3e**, **4b−c**, and **4e**) reveal different coordination geometries around the cobalt centers. X-ray diffraction studies confirmed that, whereas **1a** acts as a bidentate *N,O*-ligand, giving an octahedral coordinated Co^{II} complex (**3a**), 3- and 4-pyridyl or 4-quinolyl ligands afford tetrahedral complexes by *N*-coordination (**3b−c**, **3e**, **4b-c**, and **4e**), exclusively. The supramolecular structures for all unsolvated complexes are dominated by nonconventional O−H···Cl hydrogen bonds. The latter chains are interrupted, partially (**5**) or totally (**3e**), whenever an oxygen containing solvent is included in the structures and giving O−H···O hydrogen bonds. In the absence of conventional O−H···Cl supramolecular chains in **3e**, π−π interactions keep molecules in a close supramolecular arrangement to that found in the nonsolvated tetrahedral complexes **3b** and **4e**. The latter suggests that both hydrogen bonds and π−π interactions compete and can be considered structure directing interactions in these complexes. It also appears that the chirality of the ligands in conjunction with the bulky carborane favors *RR/SS* alternation as a more economic packing arrangement allowing unexpectedly short Co···Co distances. In addition, **3a** shows solvent accessible channels running parallel to the hydrogen bonded chains. The solvent could be removed from **3a** with retention of crystallinity, showing that this complex is an intrinsically porous molecular material. The porosity in **3a** seems to be triggered by the self-assembly of staggered carborane fragments along the hydrogen bonding network. Thus, complex **3a** is a rare example of a porous carborane-based metal−organic molecular material where molecules are, in contrast to porous carborane-based metal−organic frameworks, interacting by noncovalent interactions. The magnetic results for **3a−c** agree well with their crystallographic data and stress the relevance of intermolecular interactions among neighboring molecules providing well-organized supramolecular 1D systems. Thus, octahedral complex **3a** is an antiferromagnetic complex with porous channels. We also show that the latter complex is able to uptake methanol vapors to convert into **3a·2MeOH**. The structure of the unsolvated compound is related to the methanol solvated compound by rotation of complex molecules within the 1D O−H···Cl hydrogen bonding networks and insertion of methanol into the network.

Finally, we show experimentally (both in solution and solid state) that the Co–OH(R) bonds in **3a** are labile and that the coordination strength of the alcohol function can be modulated by solvent assisted intermolecular hydrogen bonding. Full deprotonation of both alcohol hydrogens in the octahedral cobalt complex **3a** afforded a rare square-planar Co[II] complex **6** that has been characterized by single crystal X-ray diffraction. The square-planar geometry in this complex seems to be induced by the steric hindrance generated by the carborane moiety on the ligand. The absence of axially coordinated solvent molecules in this complex is particularly interesting from a supramolecular and coordination point of view, as the complex offers two sites for coordination. Complex **6** seems to enable O$_2$ activation, followed by transformation of the ligands and metal oxidation states affording a Co[III] carborane complex 7. We are currently exploring the reactivity of complex **6** as well as gas sorption experiments for **3a**.

The present work highlights the versatility of the coordination and supramolecular chemistry of *o*-carboranyl alcohols with cobalt and has important implications in the structure–property relationships in these compounds, in particular, and structural chemistry, in general. These observations also aid in the understanding of the basic principles of metallosupramolecular chemistry of *o*-carboranyl systems and, consequently, the progress of crystal engineering.

A number of further avenues of exploration arise from the present work: (1) Would the acceptor character of the *o*-carborane cluster have any electronic effect on the *N,O*-donor set of our ligands? (2) How would this affect the new ligands when compared to the related purely organic ligands? (3) Would it be possible to obtain polynuclear complexes of the bulky *o*-carboranyl alcohols? We are currently investigating these questions and extending the metallosupramolecular chemistry of these ligands to other transition metals.

■ EXPERIMENTAL SECTION

General Aspects. All manipulations were carried out under air unless otherwise noted. The reactions were carried out in glass vials equipped with a magnetic stirring bar and capped with a septum. Chemicals were used as follows: Ethanol and methanol were distilled from CaH$_2$; acetone was distilled from P$_2$O$_5$; and CoCl$_2$·6H$_2$O (98.9%, Fluka) was used as received. *closo-ortho*-Carboranylmethanols **1a**−**e** and **2a**−**e** were synthesized as previously reported.[5] FTIR spectra were recorded from KBr pellets or ATR on a Perkin–Elmer 1720X spectrometer. The UV–vis–NIR spectra of compounds **2a**−**c** in reflectance or absorbance mode were recorded at room temperature on a double beam spectrophotometer Varian Cary 5000 with an operational range of 190−2500 nm equipped with a Diffuse Reflectance Sphere DRA-2500 accessory. BaSO$_4$ powder was used as reflectance reference material. ^{1}H, ^{13}C{^{1}H}, and ^{11}B NMR spectra were recorded at 300, 75, and 96 MHz, respectively, on a Bruker ARX 300 MHz spectrometer and referenced to the solvent (^{1}H, residual [D$_5$]acetone; ^{13}C, [D$_6$]acetone) or BF$_3$·OEt$_2$ (^{11}B NMR). Chemical shifts (δ) are reported in ppm and coupling constants (J) in Hz; peaks are described as follows: s, singlet; d, doublet; t, triplet; sept, septet; br, broad; m, multiplet. Elemental analyses (C, H, N) were performed in the Analysis Service of the Universitat Autònoma de Barcelona on a Carlo Erba CHNS EA-1108 microanalyzer. Samples for thermogravimetric characterization were placed in open alumina crucibles and analyzed using a NETZSCH STA 449F1 thermobalance operating under nitrogen. A heating rate of 10 °C/min was used, and all samples (5−13 mg) were studied between 40 and 1000 °C. UV–visible measurements were carried out on a Hewlett-Packard 8453 diode array spectrometer equipped with a Lauda RE 207 thermostat using a screw capped quartz cuvette. X-ray powder diffraction (XRPD) data was collected on a Siemens Analytical X-ray D-5000 diffractometer with Cu Kα radiation. All XRPD measurements were carried out at room temperature.

Synthesis of Co(II) Complexes 3a−e and 4a−e. *General.* Ethanol or acetone solutions (0.25 mL) of CoCl$_2$·6H$_2$O (0.04 mmol, 9.5 mg) were added dropwise to stirred solutions (acetone) or suspensions (ethanol) of the appropriate *o*-carboranylmethanols (0.08 mmol, **1a−c**: 20.1 mg, **1d−e**: 24.1 mg; **2a-c**: 21.2 mg; **2d-e**: 25.2 mg) in the same solvents (0.25 mL). The blue solution turned bright blue in most of the cases and blue-green for complex **4d** within seconds, and in the case of ethanol, complete dissolution of the starting pyridine based ligand was also observed. The reaction mixture was stirred for 30 min and allowed to concentrate by solvent evaporation under a current of nitrogen until precipitation of complexes was observed. The crude product was then washed with a mixture of ethanol/ether (1:50) and dried under vacuum to obtain the desired complexes in high yields. Complementary *in situ* NMR experiments showed that the *o*-carboranylmethanols react immediately after they are mixed with the cobalt salt with >99% conversion into the corresponding complex, based on the free ligand signals. For such experiments, **1a−e** or **2a−e** (ca. 20.0 mg) were dissolved in [D$_6$]acetone (0.250 mL) in an NMR tube and then an [D$_6$]acetone solution with 0.5 equiv of CoCl$_2$·6H$_2$O was added at room temperature. The experiments were followed by NMR (^{1}H and ^{11}B NMR) after observing that the initial blue solution turned to bright blue.

Synthesis of cis-CoCl$_2$[(2-pyridine)(o-carboranyl)methanol]$_2$, 3a. The general procedure was followed using (2-pyridine)(*o*-carboranyl)methanol (**1a**). Complex **3a** was obtained as a light violet solid (19.4 mg, 0.031 mmol, 88%). Violet crystals suitable for X-ray diffraction determinations were obtained by slow evaporation of the solvent of the reaction mixture (acetone or ethanol) previously filtered through Celite. The violet crystals corresponding to the methanol solvate **3a·2MeOH** were obtained from a concentrated methanol solution of the complex (i.e., 0.15 M) left in a closed vial at RT during 1−2 days. ^{1}H and ^{13}C NMR spectra showed a few very broad and noisy signals. ^{11}B NMR (96 MHz, [D$_6$]acetone) δ −3.24 (br d, J = 164 Hz, 2B), −10.09 (br m, 8B). FTIR (in KBr): ν_{OH} = 3137; ν_{CH} = 3048 (cluster); ν_{CH} = 2932, 2802, 2725 2570; ν_{BH} = 2617, 2578, 2589; 1608−500 other signals. Elemental Analysis for C$_{16}$H$_{34}$B$_{20}$Cl$_2$CoN$_2$O$_2$ (M: 632.51 g/mol): calculated C 30.38%, H 5.42%, N 4.43%; found C 30.45%, H 5.34%, N 4.36%.

Synthesis of CoCl$_2$[(3-pyridine)(o-carboranyl)methanol]$_2$, 3b. The general procedure was followed using (3-pyridine)(*o*-carboranyl)methanol (**1b**). Complex **3b** is obtained as a bright blue solid (17.0 mg, 0.027 mmol, 85%). Blue crystals suitable for X-ray diffraction determinations were obtained by slow evaporation of the reaction solvent. ^{1}H NMR (300 MHz, [D$_6$]acetone): δ 148 (br s; 1H, H2), 140 (br s; 1H, H6), 41.11 (s, 1H; H5), 8.67 (s; H4),[28] 6.12 (s, 1H; OH), 4.51 (s, 1H; CHOH), 3.34 (s, 1H; C$_{cluster}$H). ^{1}H{^{11}B} NMR (300 MHz, [D$_6$]-acetone), only the new signals due to B−H protons are listed: δ 2.54 (br s, 2H), 2.11 (s, 2H), 1.86 (s, 1H), 1.63 (s, 1H), 1.46 (s, 1H), 1.35 (br s, 1H), −1.68 (br s, 1H). ^{13}C{^{1}H} NMR (75 MHz, [D$_6$]acetone): δ 534.6 (br s; C2), 526.6 (br s; C6), 282 (s; C3 or C5), 263 (s; C5 or C3), 137.80 (s; C4), 120.30 (s; CHOH), 86.90 (s; C$_{cluster}$), 62.59 (s; C$_{cluster}$). ^{11}B NMR (96 MHz, [D$_6$]acetone): δ −4.19 (d, J = 85.5 Hz, 2B), −9.41 (br s, 2B), −11.87 (br s, 2B), −13.33 (d, J = 77.0 Hz, 4B). FTIR (in KBr): ν_{OH} = 3371; ν_{CH} = 3081 (cluster); ν_{CH} = 2976, 2929, 2898, 2872; ν_{BH} = 2613, 2578; 1608−500 other signals. Elemental Analysis for C$_{16}$H$_{34}$B$_{20}$Cl$_2$CoN$_2$O$_2$·0.25ether (M: 651.04 g/mol): calculated C 31.36%, H 5.65%, N 4.30%; found C 31.88%, H 5.55%, N 4.32%.

Synthesis of CoCl$_2$[(4-pyridine)(o-carboranyl)methanol]$_2$, 3c. The general procedure was followed using (4-Ppyridine)(*o*-carboranyl)-methanol (**1c**). Complex **3c** is obtained as a bright blue solid (darker than **3b**) (19.5 mg, 0.031 mmol, 88%). Crystallization processes using different solvents and mixtures led to bright blue crystals, but they were not suitable for XRD measurements. ^{1}H NMR (300 MHz, [D$_6$]acetone): δ 146 (br s, 2H; H2, H6), 40.14 (s, 2H; H3, H5), 5.00 (br s, 1H; OH), 4.31 (s, 1H; CHOH), 3.54 (br s, 1H; C$_{cluster}$H). ^{1}H{^{11}B} NMR (300 MHz, [D$_6$]acetone), only the new signals due to B−H protons are listed: δ 1.67 (br s, 1H), 1.56 (br s, 1H), 1.47 (br s,

2H), 1.30 (br s, 1H), 1.21–1.04 (br m, 1H), 0.90 (br d, 2H), −0.85 (br s, 1H). $^{13}C\{^1H\}$ NMR (75 MHz, [D6]acetone): δ 535.47 (br s; C2, C6), 291.77 (br s; C3, C5), 130.47 (s; C4), 78.09 (s; CHOH), 75.13 (s; C$_{cluster}$), 60.59 (s, C$_{cluster}$). ^{11}B NMR (96 MHz, [D$_6$]acetone): δ −4.08 (br s, 2B), −9.44 (d, J = 77 Hz, 2B), −12.89 (br s, 6B). FTIR (in KBr): ν$_{OH}$ = 3355; ν$_{CH}$ = 3084 (cluster); ν$_{CH}$ = 2923, 2854; ν$_{BH}$ = 2588; 1615–500 other signals. Elemental Analysis for C$_{16}$H$_{34}$B$_{20}$Cl$_2$CoN$_2$O$_2$·0.5acetone (M: 661.55 g/mol): calculated C 31.77%, H 5.42%, N 4.23%; found C 31.84%, H 5.93%, N 4.43%.

Synthesis of CoCl$_2$[(2-quinoline)(o-carboranyl)methanol]$_2$, 3d. The general procedure was followed using (2-quinoline)-(o-carboranyl)methanol (**1d**). Complex **3d** was obtained as a green-blue solid (12.5 mg, 0.028 mmol, 70%). Crystallization processes using different solvents and mixtures led to the degradation of the complex into the starting material. ^1H and ^{13}C NMR data: spectra showed a few very broad and noisy signals. ^{11}B NMR (96 MHz, [D$_6$]acetone) δ −2.5 to −10.7 (very broad m). FTIR (in KBr): ν$_{OH}$ = 3388 and ~3100 (broad); ν$_{CH}$ = 3068 (cluster); ν$_{CH}$ ~2900; ν$_{BH}$ = 2576; 1636–660 other signals. Elemental Analysis for C$_{12}$H$_{19}$B$_{10}$Cl$_2$CoNO (1:1 complex, M: 431.26 g/mol): calculated C 33.42%, H 4.44%, N 3.25% and for C$_{24}$H$_{38}$B$_{20}$Cl$_2$CoN$_2$O$_2$ (1:2 complex M: 732.63 g/mol): calculated C 39.35%, H 5.23%, N 3.82%; found C 37.20%, H 5.11%, N 3.24%. Considering that the product contains ~36% of the 1:1 complex and ~64% of the 1:2, the calculated obtained values are as follows: C 37.21%, H 4.95%, N 3.61%.

Synthesis of CoCl$_2$[(4-quinoline)(o-carboranyl)methanol]$_2$, 3e. The general procedure was followed using (4-quinoline)-(o-carboranyl)methanol (**1e**). Complex **3e** is obtained as bright light blue solid (26.1 mg, 0.036 mmol, 89%). Bright light blue crystals suitable for X-ray diffraction determinations were obtained by slow evaporation of an acetone solution. ^1H NMR (300 MHz, [D$_6$]-acetone): δ 31.40 (s, 1H, N$_{AR}$–H), 19.08 (s, 1H, N$_{AR}$–H), 11.92 (very br s, 8H, N$_{AR}$–H and HDO), 9.15 (s, 1H, N$_{AR}$–H), 7.06 (s, 1H), 6.05 (m, 1H; OH), 5.95 (s, 1H; CHOH), 4.51 (s, 1H; C$_{cluster}$H). $^1H\{^{11}B\}$ NMR (300 MHz, [D$_6$]acetone), only the new signals due to B–H protons are listed: δ 2.21 (br s, 2H), 1.74 (br s, 4H), 1.46 (br s, 2H), 1.12 (s, 1H), 0.36 (s, 2H). $^{13}C\{^1H\}$ NMR (75 MHz, [D$_6$]acetone): δ 150.86 (s), 148.33 (s), 138.64 (s) for some N$_{AR}$ carbons, the rest were not observed due to the paramagnetism of the sample, 81.42 (s; CHOH), 62.25 (s; C$_{cluster}$–H) the other C$_{cluster}$ is not observed due to the low intensity. ^{11}B NMR (96 MHz, [D$_6$]acetone): δ −2.7 to −4.2 (m, 2B), −6.60 to −16.61 (m, 8B). FTIR(ATR): ν$_{OH}$ = 3390 (br); ν$_{BH}$ = 2577; 1590–650 other signals. Elemental Analysis for C$_{24}$H$_{38}$B$_{20}$Cl$_2$CoN$_2$O$_2$ (M: 732.63 g/mol): calculated C 39.35%, H 5.23%, N 3.82%; found C 40.37%, H 6.07%, N 3.37%. The calculated values considering about 0.5 molecules of acetone per complex are as follows: C 40.21%, H 5.43%, N 3.68%.

Synthesis of CoCl$_2$[(2-pyridine)(methyl-o-carboranyl)methanol]$_2$, 4a. The general procedure was followed using (2-pyridine)(methyl-o-carboranyl)methanol (**2a**). Complex **4a** was obtained as violet-blue solid (18.5 mg, 0.028 mmol, 80%). Crystallization processes using different solvents and mixtures led to the degradation of the complex into the starting material. ^1H and ^{13}C NMR data: spectra showed a few very broad and noisy signals. ^{11}B NMR (96 MHz, [D$_6$]acetone) δ 1 to −15 (m br d). FTIR (ATR): ν$_{OH}$ = 3353; ν$_{CH}$ = 3031, 3032; ν$_{BH}$ = 2672, 2628, 2594, 2568, 2546; 1593–500 other signals. Elemental Analysis for C$_{18}$H$_{38}$B$_{20}$Cl$_2$CoN$_2$O$_2$·1ether (M: 706.63 g/mol): calculated C 33.99%, H 6.28%, N 3.96%; found C 33.48%, H 6.05%, N 3.80%.

Synthesis of CoCl$_2$[(3-pyridine)(methyl-o-carboranyl)methanol]$_2$, 4b. The general procedure was followed using (3-pyridine)(methyl-o-carboranyl)methanol (**2b**). Complex **4b** is obtained as a bright light blue solid (22.9 mg, 0.035 mmol, 87%). Crystallization processes using different solvents and mixtures led to the degradation of the complex into the starting material. ^1H NMR (300 MHz, [D$_6$]acetone): δ 151.16–132.90 (m, 2H; 1H, H6), 40.70 (s, 1H; H5), 8.54 (s, 1H, H4), 5.78 (s, 1H, OH), 5.33 (s, 4H, HDO), 3.56 (s, 1H, CHOH), 2.62 (s, 3H, CH$_3$). $^1H\{^{11}B\}$ NMR (300 MHz, [D$_6$]acetone), only the new signals due to B–H protons are listed: δ 2.48 (s, 2H), 2.36 (s, 3H), 1.33 (s, 2H), 1.20 (s, 2H), −2.41 (s, 1H). $^{13}C\{^1H\}$ NMR (75 MHz,

[D$_6$]acetone): δ 525.76 and 297 (very br s), 136.25 (s), and 122.14 (s) N$_{AR}$ carbons, 91.11 (s, CHOH), 79.00 (s, C$_{cluster}$), 64.11 (s, C$_{cluster}$), 25.00 (s, CH$_3$). ^{11}B NMR (96 MHz, [D$_6$]acetone): δ −2.45 (d, J = 139.9 Hz, 2B), −6.19 (d, J = 207.6 Hz, 2B), −6.64 to −14.43 (m, 4B). FTIR (in KBr): ν$_{OH}$ = 3356; ν$_{CH}$ = 2962, 2910, 2858; ν$_{BH}$ = 2579(b); 1608–500 other signals. Elemental Analysis for C$_{18}$H$_{38}$B$_{20}$Cl$_2$CoN$_2$O$_2$ (M: 660.57 g/mol): calculated C 32.73%, H 5.80%, N 4.24%; found C 32.58%, H 5.89%, N 4.22%.

Synthesis of CoCl$_2$[(4-pyridine)(methyl-o-carboranyl)methanol]$_2$, 4c. The general procedure was followed using (4-pyridine)(methyl-o-carboranyl)methanol (**2c**). Complex **4c** is obtained as a bright blue solid (23.7 mg, 0.036 mmol, 90%). Blue crystals suitable for X-ray diffraction determinations were obtained by slow evaporation of the reaction solvent. For this complex, it was possible to obtain crystals using acetone or ethanol, and in both cases **4c** crystallized as a solvate. ^1H NMR (300 MHz, [D$_6$]acetone): δ 146.20 (br s, 2H; H3, H5), 40.98 (s, 2H; H2, H6), 5.93 (br s, 4H; HDO), 5.29 (br s, 1.3H; OH), 5.05 (s, 1H; CH), 2.66 (s, 2.6H; C$_{cluster}$Me). $^1H\{^{11}B\}$ NMR (300 MHz, [D$_6$]acetone), only the new signals due to B–H protons are listed: δ 1.67 (br s, 1H), 1.56 (br s, 1H), 1.47 (br s, 2H), 1.30 (br s, 1H), 1.21–1.04 (br m, 1H), 0.90 (br d, 2H), −0.85 (br s, 1H). ^{13}C NMR (75 MHz, [D$_6$]acetone): δ 527.13 (br s; C3, C5), 286.04 (br s; C2, C6), 131.72 (s; C1), 78.75 (s; C$_{cluster}$Me), 77.07 (s; C$_{cluster}$), 75.26 (s, CHOH), 24.43 (s, Me). ^{11}B NMR (96 MHz, acetone): δ −3.40 (br s, 2B), −6.93 (d, 2B), −11.6 (br s, 6B). FTIR (ATR): ν$_{OH}$ = 3390, 3234; ν$_{CH}$ = 3089, 2933, 2816; ν$_{BH}$ = 2572(b); 1693–500 other signals. Elemental Analysis for C$_{18}$H$_{38}$B$_{20}$Cl$_2$CoN$_2$O$_2$ (M: 660.57 g/mol): calculated C 32.73%, H 5.80%, N 4.24%; found C 32.97%, H 5.77%, N 3.84%.

Synthesis of CoCl$_2$[(2-quinoline)(methyl-o-carboranyl)methanol], 4d. The general procedure was followed using (2-quinoline)(methyl-o-carboranyl)methanol (**2d**). Complex **4d** was obtained as green-brown solid (12.5 mg, 0.028 mmol, 70%). Crystallization processes using different solvents and mixtures led to the degradation of the complex into the starting material. Elemental analysis confirmed that the stechiometry of the complex corresponds to 1:1 assuming a tetrahedral geometry. ^1H and ^{13}C NMR data: spectra showed a few very broad and noisy signals. ^{11}B NMR (96 MHz, [D$_6$]acetone) δ −2.24 (d, J = 146.6 Hz, 1B), −5.06 (d, J = 157.6 Hz, 1B), −8.86 (m, 8B). FTIR (in KBr): ν$_{OH}$ = 3523 and 3399; ν$_{CH}$ = 3100 (cluster); ν$_{BH}$ = 2583; 1620–500 other signals. Elemental Analysis for C$_{13}$H$_{21}$B$_{10}$Cl$_2$CoNO (1:1 complex, M: 445.26 g/mol): calculated C 35.07%, H 4.75%, N 3.15%; found C 34.98%, H 4.76%, N 3.15%.

Synthesis of CoCl$_2$[(4-quinoline)(methyl-o-carboranyl)methanol]$_2$, 4e. The general procedure was followed using (4-quinoline)(methyl-o-carboranyl)methanol (**2e**). Complex **3e** is obtained as a bright blue-green solid (27.1 mg, 0.036 mmol, 89%). Aquamarine crystals suitable for X-ray diffraction determinations were obtained by slow evaporation of an acetone solution. ^1H NMR (300 MHz, [D$_6$]acetone): δ 108.16 (s, 1H, N$_{AR}$–H), 28.78 (s, 1H, N$_{AR}$–H), 18.02 (s, 1H), 10.00 (br s, 7H, HDO), 7.05 (s, 2H, N$_{AR}$–H), 6.19 (s, 1H, OH), 5.65 (s, 1H, CHOH), 1.83 (3H, CH$_3$). $^1H\{^{11}B\}$ NMR (300 MHz, [D$_6$]acetone), only the new signals due to B–H protons are listed: δ 2.70 (s, 2H), 1.76 (s, 2H), 1.51 (s, 1H), 1.30 (s, 1H), 0.88 (br s, 1H), −0.16 (br s, 1H). $^{13}C\{^1H\}$ NMR (75 MHz, [D$_6$]acetone): δ 165.62 (s), 146.84 (s), 144.92 (s), and 140.05 (s) N$_{AR}$ carbons, 83.41 (s; CHOH), 76.10 (s; C$_{cluster}$), 67.93 (s; C$_{cluster}$), 25.1 (s, CH$_3$). ^{11}B NMR (96 MHz, [D$_6$]acetone): δ −3.5 (m, 2B), −9.41 (br s, 2B), −10 (m, 8B). FTIR (ATR): ν$_{OH}$ = 3520 and 3390; ν$_{CH}$ = 3159–2996; ν$_{BH}$ = 2617, 2576(b); 1576–500 other signals. Elemental Analysis for C$_{26}$H$_{42}$B$_{20}$Cl$_2$CoN$_2$O$_2$ (M: 760.68 g/mol): calculated C 41.05%, H 5.57%, N 3.68%; found C 40.72%, H 5.78%, N 3.29%.

Synthesis of CoCl$_2$[(4-Pyridine)(o-carboranyl)methanol]$_4$, 5. An acetone solution (0.25 mL) of CoCl$_2$ anhydrous (0.04 mmol, 5.2 mg) was added dropwise to a stirred acetone solution (0.25 mL) of ligand **2c** (0.1 mmol, 25.1 mg). The blue solution turned bright blue. After ca. 30 min the solvent was partially evaporated and left at 5°. Light pink plates suitable for XRD analysis were collected after one week. NMR experiments were run in a reaction performed *in situ* in the NMR tube. ^1H NMR (300 MHz, [D$_6$]acetone): δ 70.07 (br s, ~2H;

H2, H6), 22.19 (s, ~2H; H3, H5), 5.74 (br s, 1H; OH), 4.92 (s, 1H; CHOH), 4.20 (br s, 1H; $C_{cluster}H$), 3.77 (drs, HDO). $^1H\{^{11}B\}$ NMR (300 MHz, [D_6]acetone), only the new signals due to B−H protons are listed: 2.00 (br s, 1H), 1.88 (br s, 2H), 1.80 (br s, 2H), 1.69 (br m, 2H), 1.58 (br d, 2H), 0.36 (br s, 1H). $^{13}C\{^1H\}$ NMR (75 MHz, [D_6]acetone): δ 312.01 (br s; C2, C6), 216.91 (br s; C3, C5), 141.04 (s; C4), 77.88 (s; CHOH), 75.50 (s; $C_{cluster}$), 60.74 (s, $C_{cluster}$). ^{11}B NMR (96 MHz, [D_6]acetone): δ −3.54 (2B), −9.93 (m, 8B).

Synthesis of Complex 6 and Its Oxidation to 7. Under inert atmosphere, a freshly distilled methanol solution of Bu^tOK (7.1 mg, 0.063 mmol in 0.3 mL) was added to a methanol solution of **4a** (20 mg, 0.032 mmol, in 0.3 mL). The initial pink solution turned red after the addition of the base and then darkened until obtainment of a final red wine color. Then, a fine white solid corresponding to KCl was observed and separated from the reaction mixture by centrifugation. After partial evaporation of the solvent, complex **6** was obtained from the supernatant as a light violet solid. The product was separated by centrifugation and washed with water to discard possible soluble salt impurities (0.019 mmol, 10.7 mg, 60%). FTIR (ATR): ν_{CH} = 3070; ν_{BH} = 2568; 1604−500 other signals. Complex **7** was obtained by leaving complex **6** in acetone solution for several days or weeks under air. Bright blue crystals suitable for X-ray diffraction studies were obtained for **7**. Several attempts repeatedly gave a few such a crystals after a long time in solution, which accounts for the slow oxidation process. Three X-ray determinations on such blue crystals from different reactions confirmed them to be **7**.

UV−Visible Experiments for 3a. The temperature dependent equilibrium involving octahedral and tetrahedral species derived from **3a** was monitored by UV−visible spectrophotometry. A methanol solution of the complex was placed in a screw capped cuvette, and the spectra were taken at different temperatures (form 75° to 5°). Visible bands around 535 nm are associated with an octahedral geometry, and the bands around 664 nm are associated with a tetrahedral one. The electronic spectrum of the deep blue solution of **3a** in acetone was recorded in order to confirm the presence of the peaks associated with a tetrahedral geometry.[29]

Transformation of 3a into 3a·2MeOH. A polycrystalline dry sample of complex **3a** (100 mg) was exposed to vapors of methanol for 7 days. The quantitative formation of **3a·2MeOH** was assessed by comparing the X-ray powder diffraction pattern of the crystalline product with the spectrum calculated on the basis of the single-crystal structure.

Single Crystal Studies. Single crystal intensity data for **3a**, **3b**, **3e**, **4c**, **4e**, **5**, and **6** were collected at 120 K on a Bruker Nonius KappaCCD area detector mounted at the window of a rotating Mo anode (λ(Mo Ka) = 0.71073 Å) (Table S2 of the Supporting Information). Data collection and processing were performed using the programs COLLECT[30] and DENZO,[31] and a multiscan absorption correction was applied using SADABS.[32] Data for **3a·MeOH** and **7** were collected at 100 K on a Rigaku AFC12 goniometer equipped with an enhanced sensitivity (HG) Saturn724+ detector mounted at the window of an FR-E+ SuperBright molybdenum rotating anode generator (λ(Mo Ka) = 0.71073 Å) with HF Varimax optics (100 μm focus). Data collection and processing, including a multiscan absorption correction, were performed using CrystalClear.[33] The structures were solved via direct methods[34] and refined by full matrix least-squares[35] on F^2. **3a** contains solvent accessible voids of ca. 192 Å^3 that consist of well-defined channels running along the c axis; electron density difference maps show these contain disordered solvent (probably ethanol) that was treated using the Squeeze algorithm.[36] **3b** exhibits probable rotational disorder of the carborane cage, resulting in excessively anisotropic thermal parameters; isotropic restraints were applied. The crystal quality of **4c** was poor, and voids contained many small electron density peaks that could not be adequately modeled as solvent and were treated using the Squeeze algorithm.[35] In **4e**, one of the carborane cages is disordered, and similarity restraints, with reference to the first molecule, were applied to the geometry and thermal parameters. The crystals of **5** were nonmerohedrally twinned, and attempts at deconvolution failed.

Magnetic Determinations. Magnetic susceptibility measurements of **3a** were performed between 2 and 300 K and carried out in a SQUID magnetometer Quantum Design Magnetometer, model MPMP, at the "Unitat de Mesures Magnètiques (Universitat de Barcelona)". Two different magnetic fields were used for **3a**, 0.03 T (2−30 K) and 1.0 T (2−300 K), with superimposable graphs. **3b** and **3c** were measured between 5 and 300 K using a 0.05 T field in a SQUID magnetometer model MPMS XL-7T at the ICMAB Low Temperatures and Magnetometry Service Laboratory. Pascal's constants were used to estimate the diamagnetic corrections for all three compounds **3a**−**3c**.

■ ASSOCIATED CONTENT

Ⓢ Supporting Information

Spectroscopic, crystallographic, and magnetic data. This material is available free of charge via the Internet at http://pubs.acs.org.

■ AUTHOR INFORMATION

Corresponding Author
*E-mail: jginerplanas@icmab.es.

Notes

The authors declare no competing financial interest.

■ REFERENCES

(1) Sanchez, C.; Shea, K. J.; Kitagawa, S. *Chem. Soc. Rev.* **2011**, 471.
(2) See for example: (a) Constable, E. C. *Coord. Chem. Rev.* **2008**, *252*, 842. (b) Cooke, M. W.; Chartrand, D.; Hanan, G. S. *Coord. Chem. Rev.* **2008**, *252*, 903. (c) Braga, D.; Brammer, L.; Champness, N. R. *CrystEngComm* **2005**, *7*, 1. (d) Brammer, L. *Chem. Soc. Rev.* **2004**, *33*, 476. (e) Biradha, K. *CrystEngComm* **2003**, *5*, 374. (f) Navarro, J. A. R.; Lippert, B. *Coord. Chem. Rev.* **2001**, *222*, 219. (g) Swiegers, G. F.; Malefetse, T. F. *Chem. Rev.* **2001**, *100*, 3483. (h) Holliday, B. J.; Mirkin, C. A. *Angew. Chem., Int. Ed.* **2001**, *40*, 2022. (i) Blake, A. J.; Champness, N. R.; Hubberstey, P.; Li, W.-S.; Withersby, A.; Schröder, M. *Coord. Chem. Rev.* **1999**, *183*, 117.
(3) See for example: (a) Teo, P.; Hor, T. S. A. *Coord. Chem. Rev.* **2011**, *255*, 273−28. (b) Sun, H.-L.; Wang, Z.-M.; Gao, S. *Coord. Chem. Rev.* **2010**, *254*, 1081. (c) Steed, J. W.; Atwood, J. L., *Supramolecular Chemistry*, 2nd edition, Wiley, Chichester, 2009. (d) Férey, G. *Chem. Soc. Rev.* **2008**, 37, 191−214. (e) Chi, Y-; Chou, P.-T. *Chem. Soc. Rev.* **2007**, 36, 1421−1431. (f) Robin, A. Y.; Fromm, K. M. *Coord. Chem. Rev.* **2006**, *250*, 2127−2157.
(4) Sarmah, B. J.; Dutta, D. K. *Cryst. Growth Des.* **2009**, 9, 1643 and references there in.
(5) For recent examples on metal complexes of 2-, 3- or 4-(hydroxymethyl)pyridine: for 2-; (a) Pattacini, R.; Teo, P.; Zhang, J.; Lan, Y.; Powell, A. K; Nehrkorn, J.; Waldmann, O.; Hor, T. S. A.; Braunstein, P. *Dalton Trans.* **2011**, *40*, 10526. (b) Taguchi, T.; Wernsdofer, W.; Abboud, K. A.; Christou, G. *Inorg. Chem.* **2010**, *49*, 10579. (c) Hubrich, M.; Peukert, M.; Seichter, W.; Weber, E. *Polyhedron* **2010**, *29*, 1854. (d) Telfer, S. G.; Parker, N. D.; Kuroda, R.; Harada, T.; Lefebvre, J.; Leznoff, D. B. *Inorg. Chem.* **2008**, *47*, 209. (e) Yilmaz, V. T.; Hamamci, S.; Thone, C. *Polyhedron* **2004**, *23*, 841. (f) Ito, M.; Onaka, S. *Inorg. Chim. Acta* **2004**, *357*, 1039. For 3- and/or 4-; (g) Jakab, N. I.; Vaskova, Z.; Moncol, J.; Gyurcsik, B.; Sima, J.;

Koman, M.; Valigura, D. *Polyhedron* **2010**, *29*, 2262. (h) Murugavel, R.; Kuppuswamy, S.; Gogoi, N.; Boomishankar, R.; Steiner, A. *Chem.—Eur. J.* **2010**, *16*, 994. (i) Bacchi, A.; Carcelli, M.; Chiodo, T.; Mezzadri, F. *CrystEngComm* **2008**, *10*, 1916.

(6) (a) Deb, B.; Sarmah, P. P.; Dutta, D. K. *Eur. J. Inorg. Chem.* **2010**, 1710. (b) Crassous, J. *Chem. Soc. Rev.* **2009**, *38*, 830.

(7) (a) Terrasson, V.; Planas, Prim, D.; Viñas, C.; J., G.; Teixidor, F.; Light, M. E.; Hursthouse, M. B. *J. Org. Chem.* **2008**, *73*, 9140. (b) Terrasson, V.; García, Y.; Farràs, P.; Teixidor, F.; Viñas, C.; Planas, J. G.; Prim, D.; Light, M. E.; Hursthouse, M. B. *CrystEngComm.* **2010**, *12*, 4109. (c) Di Salvo, F.; Planas, J. G.; Camargo, B.; Garcia, Y.; Teixidor, F.; Viñas, C.; Light, M. E.; Hursthouse, M. B. *CrystEngComm* **2011**, *13*, 5788.

(8) See for example: (a) Fontanet, M.; Popescu, A.-R.; Fontrodona, X.; Rodriguez, M.; Romero, I.; Teixidor, F.; Viñas, C.; Aliaga-Alcalde, N.; Ruiz, E. *Chem.—Eur. J.* **2011**, *17*, 13217. (b) Spokoyny, A. M.; Machan, C. W.; Clingerman, D. J.; Rosen, M. R.; Wiester, M. J.; Kennedy, R. D.; Stern, C. L.; Sarjeant, A. A.; Mirkin, C. A. *Nature Chem.* **2011**, *3*, 590. (c) Terrasson, V.; Planas, J. G.; Viñas, C.; Teixidor, F.; Prim, D.; Light, M. E.; Hursthouse, M. B. *Organometallics* **2010**, *29*, 4130. (d) Nunez, R.; Farras, P.; Teixidor, F.; Vinas, C.; Sillampaa, R.; Kivekas, R. *Angew. Chem., Int. Ed.* **2006**, *45*, 1270. (e) Teixidor, F.; Barbera, G.; Vaca, A.; Kivekas, R.; Sillampaa, R.; Oliva, J.; Vinas, C. *J. Am. Chem. Soc.* **2005**, *127*, 10158. (f) Grimes, R. N. *J. Chem. Educ.* **2004**, *81*, 657. (g) Teixidor, F; Viñas, C.; Demonceau, A.; Nuñez, R. *Pure Appl. Chem.* **2003**, *75*, 1305. (h) Teixidor, F.; Nunez, R.; Vinas, C.; Sillampaa, R.; Kivekas, R. *Angew. Chem., Int. Ed.* **2000**, *39*, 4290. (i) Plesek, J. *Chem. Rev.* **1992**, *92*, 269. (j) Bregadze, V. I. *Chem. Rev.* **1992**, *92*, 209.

(9) (a) Britovsek, G. J. P.; Bruce, M.; Gibson, V. C.; Kimberley, B. S.; Maddox, P. J.; Mastroianni, S.; McTavish, S. J.; Redshaw, C.; Solan, G. A.; Strömberg, S.; White, A. J. P.; Williams, D. J. *J. Am. Chem. Soc.* **1999**, *121*, 8728. (b) Sénèque, O.; Campion, M.; Giorgi, M.; Le Mest, Y.; Reinaud, O. *Eur. J. Inorg. Chem.* **2004**, 1817.

(10) (a) Pulici, M.; Caneva, E.; Crippa, S. *J. Chem. Research (S)* **1997**, 160−161. (b) Schwarzhans, K. E. *Angew. Chem., Int. Ed.* **1970**, *9*, 946.

(11) Todd, L. J. *Progress in NMR Spectroscopy* **1979**, *13*, 87.

(12) (a) Saxena, A. K.; Maguire, J. A.; Hosmane, N. S. *Chem. Rev.* **1997**, *97*, 2421. (b) Saxena, A. K.; Hosmane, N. S. *Chem. Rev.* **1993**, *93*, 1081.

(13) Cotton, F. A.; Francia, R. *J. Am. Chem. Soc.* **1960**, *82*, 2983.

(14) (a) Karasawa, S.; Koga, N. *Inorg. Chem.* **2011**, *50*, 5186. (b) Ma, Z.; Han, S.; Kravtsov, V. C.; Moulton, B. *Inorg. Chim. Acta* **2010**, *363*, 387. (c) Hubrich, M.; Peukert, M.; Seichter, W.; Weber, E. *Polyhedron* **2010**, *29*, 1854. (d) Putzien, S.; Wirth, S.; Roedel, J. N.; Lorenz, I.-P. *Z. Anorg. Allg. Chem.* **2009**, *635*, 1100. (e) Gao, S.; Zhang, X.-F.; Huo, L.-H.; Lu, Z.-Z.; Zhao, H.; Zhao, J.-G. *Acta Crystallogr. Sect. E* **2004**, *60*, m1128. (f) Yilmaz, V. T.; Hamamci, S.; Thöne, C. *Polyhedron* **2004**, *23*, 841. (g) Yilmaz, V. T.; Guney, S.; Andac, O.; Harrison, W. T. A. *Polyhedron* **2002**, *21*, 2393.

(15) The τ_4 value is a useful geometry index for quantifying the geometry of four-coordinated complexes, with square-planar complexes having $\tau_4 = 0$ and tetrahedral ones having $\tau_4 = 1$; L. Yang, R. R.; Powell, R. P. Houser *Dalton Trans.* **2007**, 955.

(16) Allen, F. H. *Acta Crystallogr. Sect. B* **2002**, *58*, 380.

(17) (Refcodes): (COLSET), Dang, F.-F.; Wang, X.-W.; Zhou, Y.-Z.; Han, G.-P.; Yang, Q.-C. *Acta Crystallogr., Sect. E: Struct. Rep. Online* **2008**, *64*, m1486. (COMCUD) Zhang, S. H.; Ge, C. M.; Feng, C. *Acta Crystallogr., Sect. E: Struct. Rep. Online* **2008**, *64*, m1627. (GESTED), Rudolf, M. F.; Wolny, J.; Ciunik, Z.; Chmielewski, P. *J. Chem. Soc., Chem. Commun.* **1988**, 1006. (HUCGES), Li, H.-Y.; Wang, L.-J.; Wang, Q.; Zeng, Q.-F. *Acta Crystallogr., Sect. E: Struct. Rep. Online* **2009**, *65*, m1073. (IDUFUJ), Xiao, H.-L.; Jian, F.-F. *Acta Crystallogr., Sect. E: Struct. Rep. Online* **2006**, *62*, m1512. (IMIFIU), Cibian, M.; Derossi, S.; Hanan, G. S. *Dalton Trans.* **2011**, *40*, 1038. (IRONUY), ; (JEWRAF), Lin, H.-W. *Z. Kristallogr.-New Cryst. Struct.* **2006**, *221*, 485. (MADWOE), Poddel'sky, A .I.; Cherkasov, V. K.; Fukin, G. K.; Bubnov, M. P.; Abakumova, L. G.; Abakumov, G. A. *Inorg. Chim. Acta* **2004**, *357*, 3632. (PELPUS), Wang, Q.; Fang, X.-N.

Acta Crystallogr., Sect. E: Struct. Rep. Online **2006**, *62*, m1946. (SESLEI), Liu, Z.-D. *Acta Crystallogr., Sect. E: Struct. Rep. Online* **2006**, *62*, m3203. (UQESIT), Zhao, P.-S.; Song, J.; Sun, X.-J.; Du, L.; Jian, F.-F. *Jiegou Huaxue (Chin.J.Struct.Chem.)* **2011**, *30*, 346.

(18) Ma, H.; Wan, C.; Zewail, A. H. *Proc. Natl. Acad. Sci. U.S.A.* **2008**, 10512754−12757.

(19) See for example: (a) Desiraju, G. R., *Crystal Engineering. The Design of Organic Solids*, Elsevier Science Publishers B. V., Amsterdam, 1989; (b) Etter, M. C. *Acc. Chem. Res.* **1990**, *23*, 120. (c) Desiraju, G. R.; Steiner, T., *The Weak Hydrogen Bond in Structural Chemistry and Biology*, Oxford University Press, Oxford, 2001; (d) Steiner, T. *Angew. Chem.* **2002**, *114*, 50; *Angew. Chem., Int. Ed.* **2002**, *41*, 48. (e) Atwood, J. L.; Steed, J. W., *Encyclopedia of Supramolecular Chemistry*, Marcel Dekker, New York, 2004; (f) Metrangolo, P.; Neukirch, H.; Pilati, T.; Resnatti, G. *Acc. Chem. Res.* **2005**, *38*, 386. (g) Kitagawa, S.; Uemura, K. *Chem. Soc. Rev.* **2005**, *34*, 109. (h) Britz, D. A.; Khlobystov, A. N. *Chem. Soc. Rev.* **2006**, *35*, 637. (i) Steed, J. W.; Atwood, J. L., *Supramolecular Chemistry*, 2nd *edition*, Wiley, Chichester, 2009.

(20) Janiak, C. *J. Chem. Soc., Dalton Trans.* **2000**, 3885.

(21) Choudhury, R. R.; Chitra, R. *CrystEngComm* **2010**, *12*, 2113.

(22) Holst, J. R.; Trewin, A.; Cooper, A. I. *Nat. Chem.* **2010**, *2*, 915.

(23) XIYPAX: Jerzykiewcz, L. B.; Utko, J.; Sobota, P. *Acta Crys.* **2008**, *E64*, m657.

(24) Carlin, R. L. *Magnetochemistry*, Springer-Verlag, 1986.

(25) (a) Morris, R.; Wheatley, P. *Angew. Chem., Int. Ed.* **2008**, *47*, 4966. (c) Davis, M. E. *Nature* **2002**, *417*, 813. (c) Cheetham, A. K.; Férey, G.; Loiseau, T. *Angew. Chem., Int. Ed.* **1999**, *38*, 3268.

(26) (a) He, Y.; Xiang, S.; Chen, B. *J. Am. Chem. Soc.* **2011**, *133*, 14570. (b) James, S. L. *Chem. Soc. Rev.* **2003**, *32*, 276. (c) Eddaoudi, M.; Moler, D. B.; Li, H.; Chen, B.; Reineke, T. M.; O'Keeffe, M.; Yaghi, O. M. *Acc. Chem. Res.* **2001**, *34*, 319. (d) Eddaoudi, M.; Groy, T. L.; Yaghi, O. M. *J. Am. Chem. Soc.* **1998**, *120*, 8571. (e) Li, H.; Yaghi, O. M.; Davis, C. L.; Li, G.; Li, H. *J. Am. Chem. Soc.* **1997**, *119*, 2861. (f) Brunet, P.; Simard, M.; West, J. D. *J. Am. Chem. Soc.* **1997**, *119*, 2737.

(27) (a) Spokoyny, A. M.; Farha, O. K.; Mulfort, K. L.; Hupp, J. T.; Mirkin, C. A. *Inorg. Chim. Acta* **2010**, *364*, 266. (b) Bae, Y.-S.; Spokoyny, A. M.; Farha, O. K.; Snurr, R. Q.; Hupp, J. T.; Mirkin, C. A. *Chem. Commun.* **2010**, *46*, 3478. (c) Farha, O. K.; Spokoyny, A. M.; Mulfort, K. L.; Galli, S.; Hupp, J. T.; Mirkin, C. A. *Small* **2009**, *5*, 1727. (d) Farha, O. K.; Spokoyny, A. M.; Mulfort, K. L.; Hawthorne, M. F.; Mirkin, C. A.; Hupp, J. T. *J. Am. Chem. Soc.* **2007**, *129*, 12680.

(28) Signal partially overlapped with a broad resonance due to the H_2O/HDO.

(29) (a) Cotton, F. A.; Wilkinson, G.; Murillo, C. A.; Bochmann, M. *Advanced Inorganic Chemistry*, John Wiley & Sons, 1999;

(30) COLLECT data collection software, Nonius B.V., 1998.

(31) Otwinowski, Z.; Minor, W., ″ Processing of X-ray Diffraction Data Collected in Oscillation Mode ″, *Methods Enzymol.*, Vol. 276: Macromolecular Crystallography, part A, p307−326, 1997,Carter, C.W.; , Jr. & Sweet, R.M., Eds., Academic Press.

(32) Sheldrick, G. M. SADABS - Bruker area detector scaling and absorption correction, V2.10. Institut fur Anorganische Chemie der 1270 Universitat: Tammanstrasse 4, D-3400 Gottingen, Germany, 2003.

(33) *CrystalClear-SM Expert 2.0 r7*; Rigaku: 2011.

(34) Sheldrick, G. M.. *SHELX97: Programs for Crystal Structure Analysis (Release 97-2)*; Institut fur Anorganische Chemie der Universitat: Tammanstrasse 4, D-3400 Gottingen, Germany, 1998.

(35) Bruno, J.; Cole, J. C.; Edgington, P. R.; Kessler, M.; Macrae, C. F.; McCabe, P.; Pearson, J.; Taylor, R. *Acta Crystallogr.* **2002**, *B58*, 389.

(36) SQUEEZE. Sluis, P. v. d.; Spek, A. L. *Acta Crystallogr.* **1990**, *A46*, 194−201.